MIT OpenCourseWare
http://ocw.mit.edu

Haus, Hermann A., and James R. Melcher. *Electromagnetic Fields and Energy.*
Englewood Cliffs, NJ: Prentice-Hall, 1989. ISBN: 9780132490207.

Please use the following citation format:

Haus, Hermann A., and James R. Melcher, *Electromagnetic Fields and
Energy*. (Massachusetts Institute of Technology: MIT
OpenCourseWare). http://ocw.mit.edu (accessed [Date]). License:
Creative Commons Attribution-NonCommercial-Share Alike.

Also available from Prentice-Hall: Englewood Cliffs, NJ, 1989. ISBN:
9780132490207.

Note: Please use the actual date you accessed this material in your citation.

For more information about citing these materials or our Terms of Use, visit:
http://ocw.mit.edu/terms

8

MAGNETOQUASISTATIC FIELDS: SUPERPOSITION INTEGRAL AND BOUNDARY VALUE POINTS OF VIEW

8.0 INTRODUCTION

MQS Fields: Superposition Integral and Boundary Value Views

We now follow the study of electroquasistatics with that of magnetoquasistatics. In terms of the flow of ideas summarized in Fig. 1.0.1, we have completed the EQS column to the left. Starting from the top of the MQS column on the right, recall from Chap. 3 that the laws of primary interest are Ampère's law (with the displacement current density neglected) and the magnetic flux continuity law (Table 3.6.1).

$$\boxed{\nabla \times \mathbf{H} = \mathbf{J}} \tag{1}$$

$$\boxed{\nabla \cdot \mu_o \mathbf{H} = 0} \tag{2}$$

These laws have associated with them continuity conditions at interfaces. If the interface carries a surface current density $\mathbf{K}$, then the continuity condition associated with (1) is (1.4.16)

$$\mathbf{n} \times (\mathbf{H}^a - \mathbf{H}^b) = \mathbf{K} \tag{3}$$

and the continuity condition associated with (2) is (1.7.6).

$$\mathbf{n} \cdot (\mu_o \mathbf{H}^a - \mu_o \mathbf{H}^b) = 0 \tag{4}$$

In the absence of magnetizable materials, these laws determine the magnetic field intensity $\mathbf{H}$ given its source, the current density $\mathbf{J}$. By contrast with the electroquasistatic field intensity $\mathbf{E}$, $\mathbf{H}$ is not everywhere irrotational. However, it is solenoidal everywhere.

1

The similarities and contrasts between the primary EQS and MQS laws are the topic of this and the next two chapters. The similarities will streamline the development, while the contrasts will deepen the understanding of both MQS and EQS systems. Ideas already developed in Chaps. 4 and 5 will also be applicable here. Thus, this chapter alone plays the role for MQS systems taken by these two earlier chapters for EQS systems.

Chapter 4 began by expressing the irrotational **E** in terms of a scalar potential. Here **H** is not generally irrotational, although it may be in certain source-free regions. On the other hand, even with the effects of magnetization that are introduced in Chap. 9, the generalization of the magnetic flux density $\mu_o\mathbf{H}$ has no divergence anywhere. Therefore, Sec. 8.1 focuses on the solenoidal character of $\mu_o\mathbf{H}$ and develops a vector form of Poisson's equation satisfied by the vector potential, from which the H field may be obtained.

In Chap. 4, where the electric potential was used to represent an irrotational electric field, we paused to develop insights into the nature of the scalar potential. Similarly, here we could delve into the way in which the vector potential represents the flux of a solenoidal field. For two reasons, we delay developing this interpretation of the vector potential for Sec. 8.6. First, as we see in Sec. 8.2, the superposition integral approach is often used to directly relate the source, the current density, to the magnetic field intensity without the intetermediary of a potential. Second, many situations of interest involving current-carrying coils can be idealized by representing the coil wires as surface currents. In this idealization, all of space is current free except for some surfaces within which surface currents flow. But, because **H** is irrotational everywhere except through these surfaces, this means that the H field may be expressed as the gradient of a *scalar* potential. Further, since the magnetic field is divergence free (at least as treated in this chapter, which does not deal with magnetizable materials), the *scalar* potential obeys Laplace's equation. Thus, most methods developed for EQS systems using solutions to Laplace's equation can be applied to the solution to MQS problems as well. In this way, we find "dual" situations to those solved already in earlier chapters. The method extends to time-varying quasistatic magnetic fields in the presence of perfect conductors in Sec. 8.4. Eventually, in Chap. 9, we shall extend the approach to problems involving piece-wise uniform and linear magnetizable materials.

Vector Field Uniquely Specified.   A vector field is uniquely specified by its curl and divergence. This fact, used in the next sections, follows from a slight modification to the uniqueness theorem discussed in Sec. 5.2. Suppose that the vector and scalar functions $\mathbf{C}(\mathbf{r})$ and $D(\mathbf{r})$ are given and represent the curl and divergence, respectively, of a vector function **F**.

$$\nabla \times \mathbf{F} = \mathbf{C}(\mathbf{r}) \tag{5}$$

$$\nabla \cdot \mathbf{F} = D(\mathbf{r}) \tag{6}$$

The same arguments used in this earlier uniqueness proof then shows that **F** is uniquely specified provided the functions $\mathbf{C}(\mathbf{r})$ and $D(\mathbf{r})$ are given everywhere and have distributions consistent with **F** going to zero at infinity. Suppose that $\mathbf{F}_a$ and $\mathbf{F}_b$ are two different solutions of (5) and (6). Then the difference solution

$\mathbf{F}_d = \mathbf{F}_a - \mathbf{F}_b$ is both irrotational and solenoidal.

$$\nabla \times \mathbf{F}_d = 0 \tag{7}$$

$$\nabla \cdot \mathbf{F}_d = 0 \tag{8}$$

The difference solution is governed by the same equations as in Sec. 5.2. With $\mathbf{F}_d$ taken to be the gradient of a Laplacian potential, the remaining steps in the uniqueness argument are equally applicable here.

The uniqueness proof shows the importance played by the two differential vector operations, curl and divergence. Among the many possible combinations of the partial derivatives of the vector components of $\mathbf{F}$, these two particular combinations have the remarkable property that their specification gives full information about $\mathbf{F}$.

In Chap. 4, we determined a vector field $\mathbf{F} = \mathbf{E}$ given that the vector source $\mathbf{C} = 0$ and the scalar source $D = \rho/\epsilon_o$. In Secs. 8.1 we find the vector field $\mathbf{F} = \mathbf{H}$, given that the scalar source $D = 0$ and that the vector source is $\mathbf{C} = \mathbf{J}$.

The strategy in this chapter parallels that for Chaps. 4 and 5. We can again think of dividing the fields into two parts, a particular part due to the current density, and a homogeneous part that is needed to satisfy boundary conditions. Thus, with the understanding that the superposition principle makes it possible to take the fields as the sum of particular and homogeneous solutions, (1) and (2) become

$$\nabla \times \mathbf{H}_p = \mathbf{J} \tag{9}$$

$$\nabla \cdot \mu_o \mathbf{H}_p = 0 \tag{10}$$

$$\nabla \times \mathbf{H}_h = 0 \tag{11}$$

$$\nabla \cdot \mu_o \mathbf{H}_h = 0 \tag{12}$$

In sections 8.1–8.3, it is presumed that the current density is given everywhere. The resulting vector and scalar superposition integrals provide solutions to (9) and (10) while (11) and (12) are not relevant. In Sec. 8.4, where the fields are found in free-space regions bounded by perfect conductors, (11) and (12) are solved and boundary conditions are met without the use of particular solutions. In Sec. 8.5, where currents are imposed but confined to surfaces, a boundary value approach is taken to find a particular solution. Finally, Sec. 8.6 concludes with an example in which the region of interest includes a volume current density (which gives rise to a particular field solution) bounded by a perfect conductor (in which surface currents are induced that introduce a homogeneous solution).

8.1 THE VECTOR POTENTIAL AND THE VECTOR POISSON EQUATION

A general solution to (8.0.2) is

$$\boxed{\mu_o \mathbf{H} = \nabla \times \mathbf{A}} \tag{1}$$

where $\mathbf{A}$ is the *vector potential*. Just as $\mathbf{E} = -grad\Phi$ is the "integral" of the EQS equation $curl\mathbf{E} = 0$, so too is (1) the "integral" of (8.0.2). Remember that we could add an arbitrary constant to Φ without affecting $\mathbf{E}$. In the case of the vector potential, we can add the gradient of an arbitrary scalar function to $\mathbf{A}$ without affecting $\mathbf{H}$. Indeed, because $\nabla \times (\nabla\psi) = 0$, we can replace $\mathbf{A}$ by $\mathbf{A}' = \mathbf{A} + \nabla\psi$. The curl of $\mathbf{A}$ is the same as of $\mathbf{A}'$.

We can interpret (1) as the specification of $\mathbf{A}$ in terms of the assumedly known physical $\mathbf{H}$ field. But as pointed out in the introduction, to uniquely specify a vector field, both its curl and divergence must be given. In order to specify $\mathbf{A}$ uniquely, we must also give its divergence. Just what we specify here is a matter of convenience and will vary in accordance with the application. In MQS systems, we shall find it convenient to make the vector potential solenoidal

$$\nabla \cdot \mathbf{A} = 0 \qquad (2)$$

Specification of the potential in this way is sometimes called setting the gauge, and with (2) we have established the *Coulomb gauge*.

We turn now to the evaluation of $\mathbf{A}$, and hence $\mathbf{H}$, from the MQS Ampère's law and magnetic flux continuity law, (8.0.1) and (8.0.2). The latter is automatically satisfied by letting the magnetic flux density be represented in terms of the vector potential, (1). Substituting (1) into Ampère's law (8.0.1) then gives

$$\nabla \times (\nabla \times \mathbf{A}) = \mu_o \mathbf{J} \qquad (3)$$

The following identity holds.

$$\nabla \times (\nabla \times \mathbf{A}) = \nabla(\nabla \cdot \mathbf{A}) - \nabla^2 \mathbf{A} \qquad (4)$$

The reason for defining $\mathbf{A}$ as solenoidal was to eliminate the $\nabla \cdot \mathbf{A}$ term in this expression and to reduce (3) to the *vector Poisson's equation*.

$$\boxed{\nabla^2 \mathbf{A} = -\mu_o \mathbf{J}} \qquad (5)$$

The vector Laplacian on the left in this expression is defined *in Cartesian coordinates* as having components that are the scalar Laplacian operating on the respective components of $\mathbf{A}$. Thus, (5) is equivalent to three scalar Poisson's equations, one for each Cartesian component of the vector equation. For example, the z component is

$$\nabla^2 A_z = -\mu_o J_z \qquad (6)$$

With the identification of $A_z \rightarrow \Phi$ and $\mu_o J_z \rightarrow \rho/\epsilon_o$, this expression becomes the scalar Poisson's equation of Chap. 4, (4.2.2). The integral of this latter equation is the superposition integral, (4.5.3). Thus, identification of variables gives as the integral of (6)

$$A_z = \frac{\mu_o}{4\pi} \int_{V'} \frac{J_z(\mathbf{r}')}{|\mathbf{r} - \mathbf{r}'|} dv' \qquad (7)$$

and two similar equations for the other two components of $\mathbf{A}$. Reconstructing the vector $\mathbf{A}$ by multiplying (7) by $\mathbf{i_z}$ and adding the corresponding x and y components, we obtain the *superposition integral for the vector potential*.

$$\boxed{\mathbf{A}(\mathbf{r}) = \frac{\mu_o}{4\pi} \int_{V'} \frac{\mathbf{J}(\mathbf{r}')}{|\mathbf{r} - \mathbf{r}'|} dv'}$$
(8)

Remember, $\mathbf{r}'$ is the coordinate of the current density source, while $\mathbf{r}$ is the coordinate of the point at which $\mathbf{A}$ is evaluated, the observer coordinate. Given the current density everywhere, this integration provides the vector potential. Hence, in principle, the flux density $\mu_o\mathbf{H}$ is determined by carrying out the integration and then taking the curl in accordance with (1).

The theorem at the end of Sec. 8.0 makes it clear that the solution provided by (8) is indeed unique when the current density is given everywhere.

In order that $\nabla \times \mathbf{A}$ be a physical flux density, $\mathbf{J}(\mathbf{r})$ cannot be an arbitrary vector field. Because $div(curl)$ of any vector is identically equal to zero, the divergence of the quasistatic Ampère's law, (8.0.1), gives $\nabla \cdot (\nabla \times \mathbf{H}) = 0 = \nabla \cdot \mathbf{J}$ and thus

$$\nabla \cdot \mathbf{J} = 0$$
(9)

The current distributions of magnetoquasistatics must be solenoidal.

Of course, we know from the discussion of uniqueness given in Sec. 8.0 that (9) does not uniquely specify the current distribution. In an Ohmic conductor, stationary current distributions satisfying (9) were determined in Secs. 7.1–7.5. Thus, any of these distributions can be used in (8). Even under dynamic conditions, (9) remains valid for MQS systems. However, in Secs. 8.4–8.6 and as will be discussed in detail in Chap. 10, if time rates of change become too rapid, Faraday's law demands a rotational electric field which plays a role in determining the distribution of current density. For now, we assume that the current distribution is that for steady Ohmic conduction.

Two-Dimensional Current and Vector Potential Distributions.

Suppose a current distribution $\mathbf{J} = \mathbf{i_z}J_z(x, y)$ exists through all of space. Then the vector potential is z directed, according to (8), and its z component obeys the scalar Poisson equation

$$A_z = \frac{\mu_o}{4\pi} \int \frac{J_z(x', y')dv'}{|\mathbf{r} - \mathbf{r}'|}$$
(10)

But this is formally the same expression, (4.5.3), as that of the scalar potential produced by a charge distribution $\rho(x', y')$.

$$\Phi = \frac{1}{4\pi\epsilon_o} \int \frac{\rho(x', y')dv'}{|\mathbf{r} - \mathbf{r}'|}$$
(11)

It was inconvenient to integrate the above equation directly. Instead, we determined the field of a line charge from symmetry and Gauss' law and integrated the resulting expression to obtain the potential (4.5.18)

$$\Phi = -\frac{\lambda_l}{2\pi\epsilon_o} ln\left(\frac{r}{r_o}\right)$$
(12)

where r is the distance from the line charge $r = \sqrt{(x-x')^2 + (y-y')^2}$ and r_o is the reference radius. The scalar potential can thus be evaluated from the two-dimensional integral

$$\Phi = -\frac{1}{2\pi\epsilon_o} \int \int \rho(x',y')ln\left(\sqrt{(x-x')^2 + (y-y')^2}/r_o\right)dx'dy' \qquad (13)$$

The vector potential of a two-dimensional z-directed current distribution obeys the same equation and thus has a solution by analogy, after a proper interchange of parameters.

$$A_z = -\frac{\mu_o}{2\pi} \int J_z(x',y')ln\left(\sqrt{(x-x')^2 + (y-y')^2}/r_o\right)dx'dy' \qquad (14)$$

Two important consequences emerge from this derivation.

(a) Every two-dimensional EQS potential $\Phi(x,y)$ produced by a given charge distribution $\rho(x,y)$, has an MQS analog vector potential $A_z(x,y)$ caused by a current density $J_z(x,y)$ with the same spatial distribution as $\rho(x,y)$. The magnetic field follows from (1) and thus

$$\mu_o\mathbf{H} = \nabla \times \mathbf{A} = \left(\mathbf{i_x}\frac{\partial}{\partial x} + \mathbf{i_y}\frac{\partial}{\partial y}\right) \times \mathbf{i_z}A_z$$
$$= -\mathbf{i_z} \times \left(\mathbf{i_x}\frac{\partial A_z}{\partial x} + \mathbf{i_y}\frac{\partial A_z}{\partial y}\right) \qquad (15)$$
$$= -\mathbf{i_z} \times \nabla A_z$$

Therefore the lines of magnetic flux density are perpendicular to the gradient of A_z. A plot of field lines and equipotential lines of the EQS problem is transformed into a plot of an MQS field problem by interpreting the equipotential lines as the lines of magnetic flux density. *Lines of constant A_z are lines of magnetic flux.*

(b) The vector potential of a line current of magnitude i along the z direction is given by analogy with (12),

$$A_z = -\frac{\mu_o}{2\pi}i \, ln \, (r/r_o) \qquad (16)$$

which is consistent with the magnetic field $\mathbf{H} = \mathbf{i_\phi}(i/2\pi r)$ given by (1.4.10), if one makes use of the curl expression in polar coordinates,

$$\mu_o\mathbf{H} = \frac{1}{r}\frac{\partial A_z}{\partial \phi}\mathbf{i_r} - \frac{\partial A_z}{\partial r}\mathbf{i_\phi} \qquad (17)$$

The following illustrates the integration called for in (8). The fields associated with singular current distributions will be used in later sections and chapters.

Example 8.1.1.   Field Associated with a Current Sheet
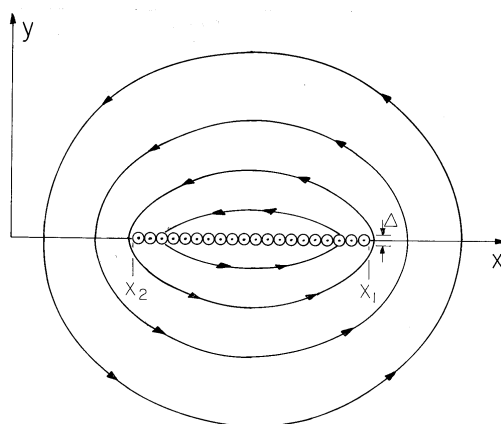
Fig. 8.1.1   Cross-section of surfaces of constant A_z and lines of magnetic flux density for the uniform sheet of current shown.

A z-directed current density is uniformly distributed over a strip located between x_2 and x_1 as shown in Fig. 8.1.1. The thickness of the sheet, Δ, is very small compared to other dimensions of interest. So, the integration of (14) in the y direction amounts to a multiplication of the current density by Δ. The vector potential is therefore determined by completing the integration on x'

$$A_z = -\frac{\mu_o K_o}{2\pi} \int_{x_2}^{x_1} ln\left(\sqrt{(x - x')^2 + y^2}/r_o\right) dx' \tag{18}$$

where $K_o \equiv J_z \Delta$.

This integral is carried out in Example 4.5.3, where the two dimensional electric potential of a charged strip was determined. Thus, with $\sigma_o/\epsilon_o \to \mu_o K_o$, (4.5.24) becomes the desired vector potential.

The profiles of surfaces of constant A_z are shown in Fig. 8.1.1. Remember, these are also the lines of magnetic flux density, $\mu_o \mathbf{H}$.

Example 8.1.2.   Two-Dimensional Magnetic Dipole Field

A pair of closely spaced conductors carrying oppositely directed currents of magnitude i is shown in Fig. 8.1.2. The currents extend to $+$ and $-$ infinity in the z direction, so the resulting fields are two-dimensional and can be represented by A_z. In polar coordinates, the distance from the right conductor, which is at a distance d from the z axis, to the observer location is essentially $r - d\cos\phi$. The A_z for each wire takes the form of (16), with r the distance from the wire to the point of observation. Thus, superposition of the vector potentials due to the two wires gives
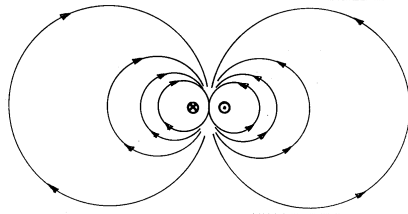
$$A_z = -\frac{\mu_o i}{2\pi}[ln(r - d\cos\phi) - lnr] = -\frac{\mu_o i}{2\pi}ln\left(1 - \frac{d}{r}\cos\phi\right) \tag{19}$$

In the limit $d \ll r$, this expression becomes

$$A_z = \mu_o \frac{id}{2\pi}\frac{\cos\phi}{r} \tag{20}$$
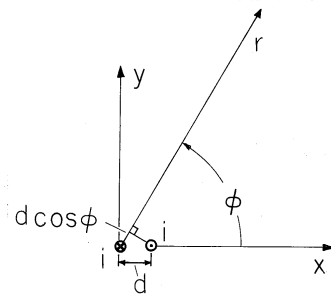
Fig. 8.1.2   A pair of wires having the spacing d carry the current i in opposite directions parallel to the z axis. The two-dimensional dipole field is shown in Fig. 8.1.3.

Fig. 8.1.3   Cross-sections of surfaces of constant A_z and hence lines of magnetic flux density for configuration of Fig. 8.1.2.

Thus, the surfaces of constant A_z have intersections with planes of constant z that are circular, as shown in Fig. 8.1.3. These are also the lines of magnetic flux density, which follow from (17).

$$\mu_o\mathbf{H} = \frac{\mu_o id}{2\pi}\left(-\frac{\sin\phi}{r^2}\mathbf{i_r} + \frac{\cos\phi}{r^2}\mathbf{i_\phi}\right) \tag{21}$$

If the line currents are replaced by line charges, the resulting equipotential lines (intersections of the equipotential surfaces with the $x - y$ plane) coincide with the magnetic field lines shown in Fig. 8.1.3. Thus, the lines of electric field intensity for the electric dual of the magnetic configuration shown in Fig. 8.1.3 originate on the positive line charge on the right and terminate on the negative line charge at the left, following lines that are perpendicular to those shown.

8.2 THE BIOT-SAVART SUPERPOSITION INTEGRAL

Once the vector potential has been determined from the superposition integral of Sec. 8.1, the magnetic flux density follows from an evaluation of *curl* $\mathbf{A}$. However, in certain field evaluations, it is best to have a superposition integral for the field itself. For example, in numerical calculations, numerical derivatives should be avoided.

The field superposition integral follows by operating on the vector potential as given by (8.1.8) before the integration has been carried out.

$$\mathbf{H} = \frac{1}{\mu_o} \nabla \times \mathbf{A} = \frac{1}{4\pi} \nabla \times \int_{V'} \left[\frac{\mathbf{J}(\mathbf{r}')}{|\mathbf{r} - \mathbf{r}'|} \right] dv' \tag{1}$$

The integration is with respect to the source coordinates denoted by $\mathbf{r}'$, while the *curl* operation involves taking derivatives with respect to the observer coordinates $\mathbf{r}$. Thus, the curl operation can be carried out before the integral is completed, and (1) becomes

$$\mathbf{H} = \frac{1}{4\pi} \int_{V'} \nabla \times \left[\frac{\mathbf{J}(\mathbf{r}')}{|\mathbf{r} - \mathbf{r}'|} \right] dv' \tag{2}$$

The *curl* operation required to evaluate the integrand in this expression can be carried out without regard for the particular dependence of the current density because the derivatives are with respect to $\mathbf{r}$, not $\mathbf{r}'$. To make this evaluation, observe that the *curl* operates on the product of the vector $\mathbf{J}$ and the scalar $\psi = |\mathbf{r} - \mathbf{r}'|^{-1}$, and that operation obeys the vector identity

$$\nabla \times (\psi \mathbf{J}) = \psi \nabla \times \mathbf{J} + \nabla \psi \times \mathbf{J} \tag{3}$$

Because $\mathbf{J}$ is independent of $\mathbf{r}$, the first term on the right is zero. Thus, (2) becomes

$$\mathbf{H} = \frac{1}{4\pi} \int_{V'} \nabla \left(\frac{1}{|\mathbf{r} - \mathbf{r}'|} \right) \times \mathbf{J} dv' \tag{4}$$

To evaluate the gradient in this expression, consider the special case when $\mathbf{r}'$ is at the origin in a spherical coordinate system, as shown in Fig. 8.2.1. Then

$$\nabla(1/r) = -\frac{1}{r^2} \mathbf{i_r} \tag{5}$$

where $\mathbf{i_r}$ is the unit vector directed from the source coordinate at the origin to the observer coordinate at (r, θ, ϕ).

We now move the source coordinate from the origin to the arbitrary location $\mathbf{r}'$. Then the distance r in (5) is replaced by the distance $|\mathbf{r} - \mathbf{r}'|$. To replace the unit vector $\mathbf{i_r}$, the *source-observer unit vector* $\mathbf{i_{r'r}}$ is defined as being *directed from an arbitrary source coordinate to the observer coordinate P*. In terms of this source-observer unit vector, illustrated in Fig. 8.2.2, (5) becomes

$$\nabla \left(\frac{1}{\mathbf{r} - \mathbf{r}'} \right) = -\frac{\mathbf{i_{r'r}}}{|\mathbf{r} - \mathbf{r}'|^2} \tag{6}$$

Substitution of this expression into (4) gives the *Biot-Savart Law* for the magnetic field intensity.

$$\boxed{\mathbf{H} = \frac{1}{4\pi} \int_{V'} \frac{\mathbf{J}(\mathbf{r}') \times \mathbf{i_{r'r}}}{|\mathbf{r} - \mathbf{r}'|^2} dv'} \tag{7}$$
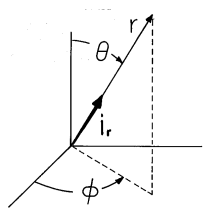
Fig. 8.2.1   Spherical coordinate system with $\mathbf{r}'$ located at origin.

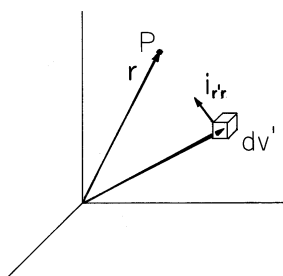**Fig. 8.2.2**   Source coordinate $\mathbf{r}'$ and observer coordinate $\mathbf{r}$ showing unit vector $\mathbf{i}_{\mathbf{r}'\mathbf{r}}$ directed from $\mathbf{r}'$ to $\mathbf{r}$.

In evaluating the integrand, the cross-product is evaluated at the source coordinate $\mathbf{r}'$. The integrand represents the contribution of the current density at $\mathbf{r}'$ *to the field at* $\mathbf{r}$. The following examples illustrate the Biot-Savart law.

Example 8.2.1.   On Axis Field of Circular Cylindrical Solenoid

The cross-section of an N-turn solenoid of axial length d and radius a is shown in Fig. 8.2.3. There are many turns, so the current i passing through each is essentially ϕ directed. To keep the integration simple, we confine ourselves to finding $\mathbf{H}$ on the z axis, which is the axis of symmetry.

In cylindrical coordinates, the source coordinate incremental volume element is $dv' = r'd\phi'dr'dz'$. For many windings uniformly distributed over a thickness Δ, the current density is essentially the total number of turns multiplied by the current per turn and divided by the area through which the current flows.

$$\mathbf{J} \cong \mathbf{i}_\phi \frac{Ni}{\Delta d} \tag{8}$$

The superposition integral, (7), is carried out first on r'. This extends from $r' = a$ to $r' = a + \Delta$ over the radial thickness of the winding. Because $\Delta \ll a$, the source-observer distance and direction remain essentially constant over this interval, and so the integration amounts to a multiplication by Δ. The axial symmetry requires that $\mathbf{H}$ on the z axis be z directed. The integration over z' and ϕ' is

$$H_z = \frac{1}{4\pi} \int_{d/2}^{-d/2} \int_0^{2\pi} \Big(\frac{Ni}{d}\Big) \frac{(\mathbf{i}_\phi \times \mathbf{i}_{r'r})_z}{|\mathbf{r} - \mathbf{r}'|^2} a d\phi' dz' \tag{9}$$

In terms of the angle α shown in Fig. 8.2.3 and its inset, the source-observer unit vector is

$$\mathbf{i}_{r'r} = -\mathbf{i_r} \sin\alpha - \mathbf{i_z} \cos\alpha \tag{10}$$
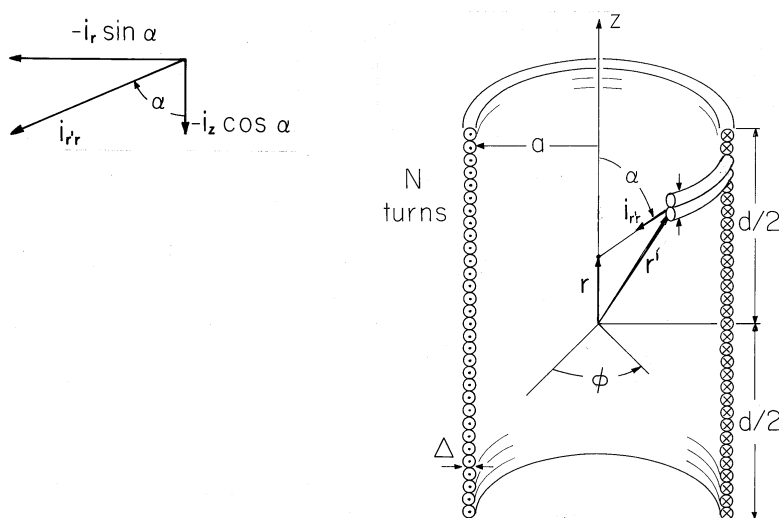
Fig. 8.2.3   A solenoid consists of N turns uniformly wound over a length d, each turn carrying a current i. The field is calculated along the z axis, so the observer coordinate is at $\mathbf{r}$ on the z axis.

so that

$$(\mathbf{i}_\phi \times \mathbf{i}_{r'r})_z = \sin \alpha = \frac{a}{\sqrt{a^2 + (z' - z)^2}}; \quad |\mathbf{r} - \mathbf{r}'|^2 = a^2 + (z' - z)^2 \tag{11}$$

The integrand in (9) is ϕ' independent, and the integration over ϕ' amounts to multiplication by 2π.

$$H_z = \frac{Ni}{2d} \int_{-d/2}^{d/2} \frac{a^2 dz'}{[a^2 + (z' - z)^2]^{3/2}} \tag{12}$$

With the substitution $z'' = z' - z$, it follows that

$$
\begin{aligned}
H_z &= \frac{Ni}{2d} \frac{z''}{\sqrt{a^2 + z''^2}} \Big]_{-\frac{d}{2} - z}^{\frac{d}{2} - z} \\
&= \frac{Ni}{2d} \left[\frac{\frac{d}{2a} - \frac{z}{a}}{\sqrt{1 + \left(\frac{d}{2a} - \frac{z}{a}\right)^2}} + \frac{\frac{d}{2a} + \frac{z}{a}}{\sqrt{1 + \left(\frac{d}{2a} + \frac{z}{a}\right)^2}} \right]
\end{aligned}
\tag{13}
$$

In the limit where $d/2a \ll 1$, the solenoid becomes a circular coil with N turns concentrated at $r = a$ in the plane $z = 0$. The field intensity at the center of this coil follows from (13) as the amp-turns divided by the loop diameter.

$$H_z \to \frac{Ni}{2a} \tag{14}$$

Thus, a 100-turn circular loop having a radius $a = 5$ cm (that is large compared to its axial length d) and carrying a current of $i = 1$ A would have a field intensity of
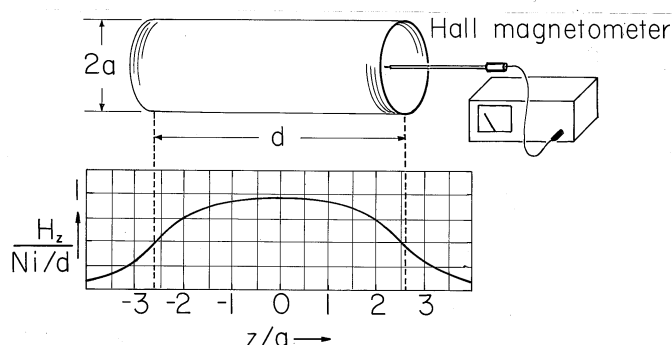
Fig. 8.2.4 Experiment for documenting the axial **H** predicted in Example 8.2.1. Profile of normalized H_z is for $d/2a = 2.58$.

1000 A/m at its center. The flux density measured by a magnetometer would then be $B_z = \mu_o H_z = 4\pi \times 10^{-7}(1000)$ tesla $= 4\pi$ gauss.

Further implications of this finding are discussed in the following demonstration.

### Demonstration 8.2.1.   Fields of a Circular Cylindrical Solenoid

The solenoid shown in Fig. 8.2.4 has $N = 141$ turns, an axial length $d = 70.5$ cm, and a radius $a = 13.6$ cm. A Hall-type magnetometer measures the magnitude and direction of **H** in and around the coil. The on-axis distribution of H_z predicted by (13) for the experimental length-to-diameter ratio $d/2a = 2.58$ is shown in Fig. 8.2.4. With $i = 1$ amp, the flux density at the center approaches 2.5 gauss. The accuracy with which theory and experiment agree is likely to be limited only by such matters as the care with which the probe can be mounted and the calibration of the magnetometer. Care must also be taken that there are no magnetizable materials, such as iron, in the vicinity of the coil. To avoid contributions from the earth's magnetic field (which is on the order of a gauss), ac fields should be used. If ac is used, there should be no large conducting objects near by in which eddy currents might be induced. (Magnetization and eddy currents, respectively, are taken up in the next two chapters.)

The infinitely long solenoid can be regarded as the analog for MQS systems of the "plane parallel plate capacitor." Just as the capacitor can be constructed to create a uniform electric field between the plates with zero field outside the region bounded by the plates, so too the long solenoid gives rise to a uniform magnetic field throughout the interior region and an exterior field that is zero. This can be seen by probing the field not only as a function of axial position but of radius as well. For the finite length solenoid, the on-axis interior field designated by H_∞ in Fig. 8.2.4 is given by (13) for locations on the z axis where $d/2 \gg z$.

$$H_z \to H_\infty \equiv \left[\frac{d/2a}{\sqrt{1 + \left(\frac{d}{2a}\right)^2}} \right] \frac{Ni}{d} \tag{15}$$

In the limit where the solenoid is also very long compared to its radius, where $d/2a \gg 1$, this expression becomes

$$H_\infty \to \frac{Ni}{d} \tag{16}$$
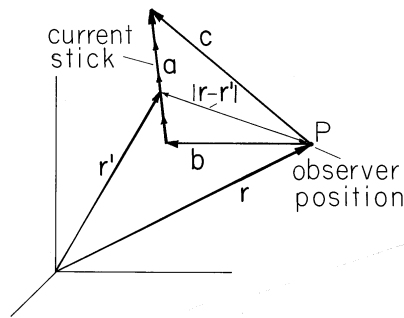
Fig. 8.2.5   A line current i is uniformly distributed over the length of the vector **a** originating at $\mathbf{r}+\mathbf{b}$ and terminating at $\mathbf{r}+\mathbf{c}$. The resulting magnetic field intensity is determined at the observer position **r**.

Probing of the field shows the field maintains the value and direction of (16) over the interior cross-section as well. It also shows that the magnetic field intensity just outside the windings at an axial location that is several radii a from the coil ends is relatively small.

Continuity of magnetic flux requires that the total flux passing through the solenoid in the z direction must be returned in the $-z$ direction outside the solenoid. How, then, can the exterior field of a long solenoid be negligible compared to that inside? The outside flux returns in the $-z$ direction through a much larger exterior area than the area πa^2 through which the interior flux passes. In fact, as the coil becomes infinitely long, this return flux spreads out over an exterior area that stretches to infinity in the x and y directions. The field intensity just outside the winding tends to zero as the coil is made very long.

Stick Model for Computing Fields of Electromagnet.   The Biot-Savart superposition integral can be completed analytically for relatively few configurations. Nevertheless, its evaluation amounts to no more than a summation of the field contributions from each of the current elements. Thus, on the computer, its evaluation is a straightforward matter.

Many practical current distributions are, or can be approximated by, connected straight-line current segments, or current "sticks." We will now use the Biot-Savart law to find the field at an arbitrary observer position **r** associated with a current stick having an arbitrary location. The result is a practical resource, because a numerical summation over differential volume current elements can then be replaced by one over the sticks.

The current stick, shown in Fig. 8.2.5, is represented by a vector **a**. Thus, the current is uniformly distributed between the base of this vector at $\mathbf{r}+\mathbf{b}$ and the tip of the vector at $\mathbf{r}+\mathbf{c}$. The source coordinate $\mathbf{r}'$ is located along the current stick. The objective in the following paragraphs is to carry out an integration over the length of the current stick and obtain an expression for $\mathbf{H}(\mathbf{r})$. Because the current stick does not represent a solenoidal current density at its ends, the field derived is of physical significance only if used in conjunction with other current sticks that together represent a continuous current distribution.

The detailed view of the current stick, Fig. 8.2.6, shows the source coordinate ξ denoting the position along the stick. The origin of this coordinate is at the point
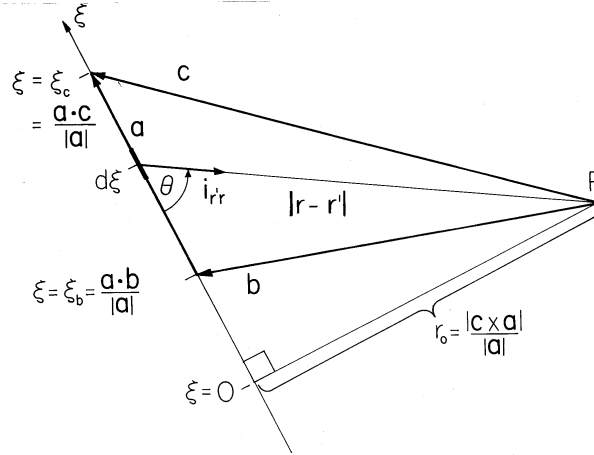
Fig. 8.2.6   View of current element from Fig. 8.2.5 in plane containing **b** and **c**, and hence **a**.

on a line through the stick that is closest to the observer coordinate.

The projection of **b** onto a vector **a** is $\xi_b = \mathbf{a} \cdot \mathbf{b}/|\mathbf{a}|$. Thus, the current stick begins at this distance from $\xi = 0$, as shown in Fig. 8.2.6, and terminates at ξ_c, the projection of **c** onto the axis of **a**, as also shown.

The cross-product $\mathbf{c} \times \mathbf{a}/|\mathbf{a}|$ is perpendicular to the plane of Fig. 8.2.6 and equal in magnitude to the projection of **c** onto a vector that is perpendicular to **a** and in the plane of Fig. 8.2.6. Thus, the shortest distance between the observer position and the axis of the current stick is $r_o = |\mathbf{c} \times \mathbf{a}|/|\mathbf{a}|$. It follows from this fact and the definition of the cross-product that

$$d\mathbf{s} \times \mathbf{i}_{r'r} = d\xi \frac{\left[\frac{\mathbf{c} \times \mathbf{a}}{|a|}\right]}{|\mathbf{r} - \mathbf{r}'|} \tag{17}$$

where $d\mathbf{s}$ is the differential along the line current and

$$|\mathbf{r} - \mathbf{r}'| = (\xi^2 + r_o^2)^{1/2}$$

Integration of the Biot-Savart law, (7), is first performed over the cross-section of the stick. The cross-sectional dimensions are small, so during this integration, the integrand remains essentially constant. Thus, the current density is replaced by the total current and the integral reduced to one on the axial coordinate ξ of the stick.

$$\mathbf{H} = \frac{i}{4\pi} \int_{\xi_b}^{\xi_c} \frac{d\mathbf{s} \times \mathbf{i}_{r'r}}{|\mathbf{r} - \mathbf{r}'|^2} \tag{18}$$

In view of (17), this integral is expressed in terms of the source coordinate integration variable ξ as

$$\mathbf{H} = \frac{i}{4\pi} \int_{\xi_b}^{\xi_c} \frac{\mathbf{c} \times \mathbf{a}\, d\xi}{|a|(\xi^2 + r_o^2)^{3/2}} \tag{19}$$
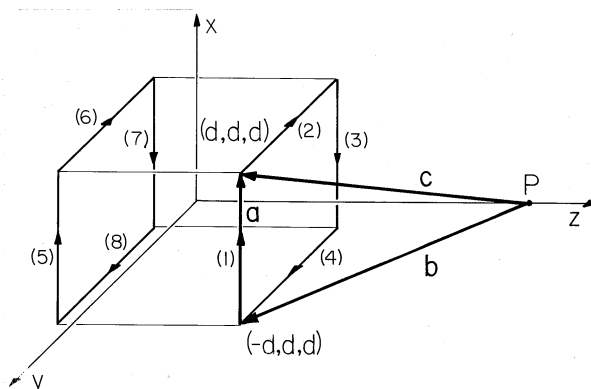
Fig. 8.2.7   A pair of square N-turn coils produce a field at P on the z axis that is the superposition of the fields H_z due to the eight linear elements comprising the coils. The coils are centered on the z axis.

This integral is carried out to obtain

$$\mathbf{H} = \frac{i}{4\pi} \frac{\mathbf{c} \times \mathbf{a}}{|a|} \left[\frac{\xi}{r_o^2[\xi^2 + r_o^2]^{1/2}} \right]_{\xi_b}^{\xi_c} \tag{20}$$

In evaluating this expression at the integration endpoints, note that by definition,

$$(\xi_c^2 + r_o^2)^{1/2} = |c|; \qquad (\xi_b^2 + r_o^2)^{1/2} = |b| \tag{21}$$

so that (20) becomes an expression for the field intensity at the observer location expressed in terms of vectors $\mathbf{a}$, $\mathbf{b}$, and $\mathbf{c}$ that serve to define the relative location of the current stick.[1]

$$\mathbf{H} = \frac{i}{4\pi} \frac{\mathbf{c} \times \mathbf{a}}{|\mathbf{c} \times \mathbf{a}|^2} \left(\frac{\mathbf{a} \cdot \mathbf{c}}{|c|} - \frac{\mathbf{a} \cdot \mathbf{b}}{|b|} \right) \tag{22}$$

The following illustrates how this expression can be used repetitively to determine the field induced by currents represented in a piece-wise fashion by current sticks. Expressed in Cartesian coordinates, the vectors are a convenient way to specify the sticks making up a complex winding. On the computer, the evaluation of (22) is then conveniently carried out by a subroutine that is used many times.

Example 8.2.2.   Axial Field of a Pair of Square Coils

Shown in Fig. 8.2.7 is a pair of coils, each having N turns carrying a current i in such a direction that the fields induced by each coil reinforce along the z axis. The four linear sections of the two coils comprise the sides of a cube, centered at the origin and with dimensions $2d$.

---

[1] Private communication, Mr. John G. Aspinall.
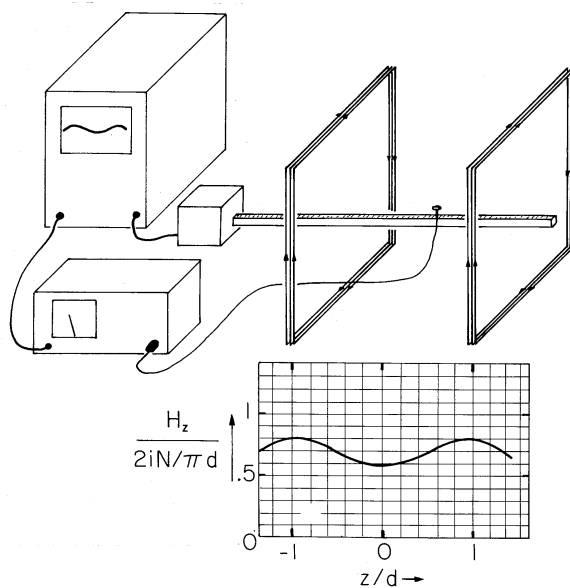
Fig. 8.2.8 Demonstration of axial field generated by pair of square coils having spacing equal to the side lengths.

We confine ourselves to finding **H** along the z axis where, by symmetry, it has only a z component. Thus, for an observer at $(0, 0, z)$, the vectors specifying element (1) of the right-hand coil in Fig. 8.2.7 are

$$\mathbf{a} = 2d\mathbf{i_x}$$

$$\mathbf{b} = -d\mathbf{i_x} + d\mathbf{i_y} + (d - z)\mathbf{i_z} \tag{23}$$

$$\mathbf{c} = d\mathbf{i_x} + d\mathbf{i_y} + (d - z)\mathbf{i_z}$$

Evaluation of the z component of (22) then gives the part of H_z due to element (1). Because of the axial symmetry, the field induced by elements (2), (3), and (4) in the same coil are the same as already found for element (1). The field induced by element (5) in the second coil is similarly found starting from vectors that are the same as in (23), except that $d \to -d$ in the z components of **b** and **c**. Here too, the other three elements each contribute the same field as already found. Thus, the axial field intensity, the sum of the contributions from the individual coils, is

$$
H_z = -\frac{2iN}{\pi d} \left\{ \frac{1}{\left[\left(1 - \frac{z}{d}\right)^2 + 1\right]\left[2 + \left(1 - \frac{z}{d}\right)^2\right]^{1/2}} \right.
$$
$$
\left. + \frac{1}{\left[\left(1 + \frac{z}{d}\right)^2 + 1\right]\left[2 + \left(1 + \frac{z}{d}\right)^2\right]^{1/2}} \right\} \tag{24}
$$

This distribution is plotted on the inset to Fig. 8.2.8. Because the fields induced by the separate coils reinforce, the pair can be used to produce a relatively uniform field in the midregion.

Demonstration 8.2.2.   Field of Square Pair of Coils

In the experiment of Fig. 8.2.8, the axial field is probed by means of a Hall magnetometer. The output is connected to the vertical trace of a high persistence scope. The probe is mounted on a carriage that is attached to a potentiometer in such a way that there is an output voltage proportional to the horizontal position of the probe. This is used to control the horizontal scope deflection. The result is a trace that follows the predicted contour. The plot is shown in terms of normalized coordinates that can be used to compare theory to experiment using any size of coils and any level of current.

8.3 THE SCALAR MAGNETIC POTENTIAL

The vector potential $\mathbf{A}$ describes magnetic fields that possess curl wherever there is a current density $\mathbf{J}(\mathbf{r})$. In the space free of current,

$$\boxed{\nabla \times \mathbf{H} = 0} \tag{1}$$

and thus $\mathbf{H}$ ought to be derivable there from the gradient of a potential.

$$\boxed{\mathbf{H} = -\nabla \Psi} \tag{2}$$

Because

$$\nabla \cdot \mu_o \mathbf{H} = 0 \tag{3}$$

we further have

$$\boxed{\nabla^2 \Psi = 0} \tag{4}$$

The potential obeys Laplace's equation.

Example 8.3.1.   The Scalar Potential of a Line Current

A line current is a source singularity (at the origin of a polar coordinate system if it is placed along its z axis). From Ampère's integral law applied to the contour C of Fig. 1.4.4, we have
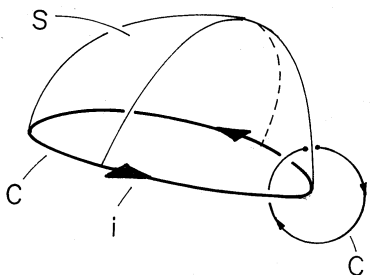
$$\oint_C \mathbf{H} \cdot d\mathbf{s} = 2\pi r H_\phi = \int_S \mathbf{J} \cdot d\mathbf{a} = i \tag{5}$$

and thus

$$H_\phi = \frac{i}{2\pi r} \tag{6}$$

It follows that the potential Ψ that has H_ϕ of (6) as the negative of its gradient is

$$\Psi = -\frac{i}{2\pi}\phi \tag{7}$$

Fig. 8.3.1   Surface spanning loop, contour following loop, and contour for $\oint \mathbf{H} \cdot d\mathbf{s}$.

Note that the potential is multiple valued as the origin is encircled more than once. This property reflects the fact that strictly, $\mathbf{H}$ is not curl free in all of space. As the origin is encircled, Ampère's integral law identifies $\mathbf{J}$ as the source of the curl of $\mathbf{H}$.

Because Ψ is a solution to Laplace's equation, it must possess an EQS analog. The electroquasistatic potential

$$\Phi = -\frac{V}{2\pi}\phi; \qquad 0 < \phi < 2\pi \tag{8}$$

describes the fringing field of a capacitor of semi-infinite extent, extending from $x = 0$ to $x = +\infty$, with a voltage V across the plates, in the limit as the spacing between the plates is negligible (Fig. 5.7.2 with V reversed in sign). It can also be interpreted as the field of a semi-infinite dipole layer with the dipole density $\pi_s = \sigma_s d = \epsilon_o V$ defined by (4.5.27), where d is the spacing between the surface charge densities, $\pm\sigma_s$, on the outside surfaces of the semi-infinite plates (Fig. 5.7.2 with the signs of the charges reversed). We now have further opportunity to relate H fields of current-carrying wires to EQS analogs involving dipole layers.

The Scalar Potential of a Current Loop.   A current loop carrying a current i has a magnetic field that is curl free everywhere except at the location of the wire. We shall now determine the scalar potential produced by the current loop. The line integral $\oint \mathbf{H} \cdot d\mathbf{s}$ enclosing the current does not give zero, and hence paths that enclose the current in the loop are not allowed, if the potential is to be single valued. Suppose that we mount over the loop a surface S spanning the loop which is not crossed by any path of integration. The actual shape of the surface is arbitrary, but the contour C_l is defined by the wire which is its edge. The potential is then made single valued. The discontinuity of potential across the surface follows from Ampère's law

$$\int_C \mathbf{H} \cdot d\mathbf{s} = i \tag{9}$$

where the broken circle on the integral sign is to indicate a path as shown in Fig. 8.3.1 that goes from one side of the surface to a point on the opposite side. Thus, the potential Ψ of a current loop has the discontinuity

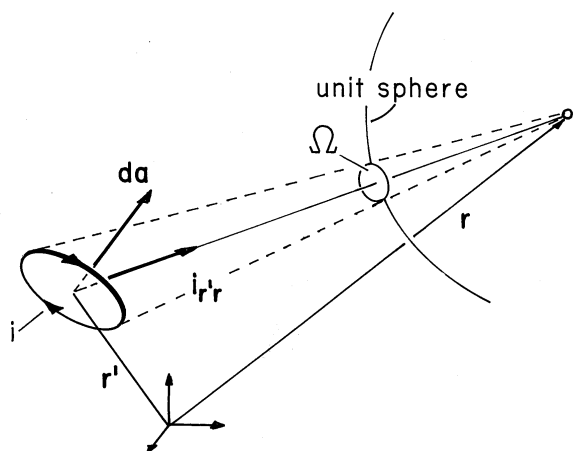$$\int \mathbf{H} \cdot d\mathbf{s} = \int (-\nabla\Psi) \cdot d\mathbf{s} = \Delta\Psi = i \tag{10}$$

Fig. 8.3.2   Solid angle for observer at **r** due to current loop at **r**′.

We have found in electroquasistatics that a uniform dipole layer of magnitude π_s on a surface S produces a potential that experiences a constant potential jump π_s/ϵ_o across the surface, (4.5.31). Its potential was (4.5.30)

$$\Phi(\mathbf{r}) = \frac{\pi_s}{4\pi\epsilon_o}\Omega \tag{11}$$

where Ω is the solid angle subtended by the rim of the surface as seen by an observer at the point **r**. Thus, we conclude that the scalar potential Ψ, a solution to Laplace's equation with a constant jump i across the surface S spanning the wire loop, must have a potential jump $\pi_s/\epsilon_o \rightarrow i$, and hence the solution

$$\boxed{\Psi(\mathbf{r}) = \frac{i}{4\pi}\Omega} \tag{12}$$

where again the solid angle is that subtended by the contour along the wire as seen by an observer at the point **r** as shown by Fig. 8.3.2. In the example of a dipole layer, the surface S specified the physical distribution of the dipole layer. In the present case, S is arbitrary as long as it spans the contour C of the wire. This is consistent with the fact that the solid angle Ω is invariant with respect to changes of the surface S and depends only on the geometry of the rim.

Example 8.3.2.   The H Field of Small Loop

Consider a small loop of area a at the origin of a spherical coordinate system with the normal to the surface parallel to the z axis. According to (12), the scalar potential of the loop is then

$$\Psi = \frac{i}{4\pi}\frac{\mathbf{i}_r \cdot \mathbf{i}_z a}{r^2} = \frac{ia}{4\pi}\frac{\cos\theta}{r^2} \tag{13}$$

This is the potential of a dipole. The H field follows from using (2)

$$\mathbf{H} = -\nabla\Psi = \frac{ia}{4\pi r^3}[2\cos\theta\mathbf{i}_r + \sin\theta\mathbf{i}_\theta] \tag{14}$$

As far as its field around and far from the loop is concerned, the current loop can be viewed as if it were a "magnetic" dipole, consisting of two equal and opposite magnetic charges $\pm q_m$ spaced a distance d apart (Fig. 4.4.1 with $q \to q_m$). The magnetic charges (monopoles) are sources of divergence of the magnetic flux $\mu_o\mathbf{H}$ analogous to electric charges as sources of divergence of the displacement flux density $\epsilon_o\mathbf{E}$. Thus, if Maxwell's equations are modified to include the action of a magnetic charge density

$$\rho_m = \lim_{\Delta V \to 0} \frac{q_m}{\Delta V}$$

in units of voltsec/m^4, then the new magnetic Gauss' law must be

$$\nabla \cdot \mu_o\mathbf{H} = \rho_m \tag{15}$$

in analogy with

$$\nabla \cdot \epsilon_o\mathbf{E} = \rho \tag{16}$$

Now, magnetic monopoles have been postulated by Dirac, and recent searches for the existence of such monopoles have been apparently successful[2]. Because the search is so difficult, it is apparent that, if they exist at all, they are very rare in nature. Here the introduction of magnetic charge is a matter of convenience so that the field produced by a small current loop can be pictured as the field of a *magnetic dipole*. This can serve as a mnemonic for the reconstruction of the field. Thus, if it is remembered that the potential of the electric dipole is

$$\Phi = \frac{\mathbf{p} \cdot \mathbf{i_{r'r}}}{4\pi\epsilon_o|\mathbf{r} - \mathbf{r'}|^2} \tag{17}$$

the potential of a magnetic dipole can be easily recalled as

$$\Psi = \frac{\mathbf{p}_m \cdot \mathbf{i_{r'r}}}{4\pi\mu_o|\mathbf{r} - \mathbf{r'}|^2} \tag{18}$$

where

$$p_m \equiv q_m d = \mu_o ia = \mu_o m \tag{19}$$

The magnetic dipole moment is defined as the product of the magnetic charge, q_m, and the separation, d, or by μ_o times the current times the area of the current loop. Another symbol is used commonly for the "dipole moment" of a current loop, $m \equiv ia$, the product of the current times the area of the loop without the factor μ_o. The reader must gather from the context whether the words dipole moment refer to p_m or $m = p_m/\mu_o$. The magnetic field intensity $\mathbf{H}$ of a magnetic dipole at the origin, (14), is

$$\mathbf{H} = -\nabla\Psi = \frac{m}{4\pi r^3}(2\cos\theta\mathbf{i_r} + \sin\theta\mathbf{i}_\theta) \tag{20}$$

Of course, the details of the field produced by the current loop and the magnetic charge-dipole differ in the near field. One has $\nabla \cdot \mu_o\mathbf{H} \neq 0$, and the other has a solenoidal $\mathbf{H}$ field.

---

[2] *Science* Vol. 216, (June 4, 1982).

## 8.4 MAGNETOQUASISTATIC FIELDS IN THE PRESENCE OF PERFECT CONDUCTORS

There are physical situations in which the current distribution is not prespecified but is given by some equivalent information. Thus, for example, a *perfectly conducting* body in a time-varying magnetic field supports surface currents that shield the **H** field from the interior of the body. The effect of the conductor on the magnetic field is reminiscent of the EQS situations of Sec. 4.6, where charges distributed themselves on the surface of a conductor in such a way as to shield the electric field out of the material.

We found in Chap. 7 that the EQS model of a perfect conductor described the low-frequency response of systems in the sinusoidal steady state, or the long-time response to a step function drive. We will find in Chap. 10 that the MQS model of a perfect conductor represents the high-frequency sinusoidal steady state response or the short-time response to a step drive.

Usually, we use the model of perfect conductivity to describe bodies of high but finite conductivity. The value of conductivity which justifies use of the perfect conductor model depends on the frequency (or time scale in the case of a transient) as well as the geometry and size, as will be seen in Chap. 10. When the material is cooled to the point where it becomes superconducting, a type I superconductor (for example lead) expels any mangetic field that might have originally been within its interior, while showing zero resistance to currrent flow. Thus, even for dc, the material acts on the magnetic field like a perfect conductor. However, type I materials also act to exclude the flux from the material, so they should be regarded as perfect conductors in which flux cannot be trapped. The newer "high temperature ceramic superconductors," such as $Y_1Ba_2Cu_3O_7$, show a type II regime. In this class of superconductors, there can be trapped flux if the material is cooled in a dc field. "High temperature superconductors" are those that show a zero resistance at temperatures above that of liquid nitrogen, 77 degrees Kelvin.

As for EQS systems, Faraday's continuity condition, (1.6.12), requires that the tangential **E** be continuous at a boundary between free space and a conductor. By definition, a stationary perfect conductor cannot have an electric field in its interior. Thus, in MQS as well as EQS systems, there can be no tangential **E** at the surface of a perfect conductor. But the primary laws determining **H** in the free space region, Ampère's law with **J** = 0 and the flux continuity condition, do not involve the electric field. Rather, they involve the magnetic field, or perhaps the vector or scalar potential. Thus, it is desirable to also state the boundary condition in terms of **H** or Ψ.

Boundary Conditions and Evaluation of Induced Surface Current Density. To identify the boundary condition on the magnetic field at the surface of a perfect conductor, observe first that the magnetic flux continuity condition requires that if there is a time-varying flux density $\mathbf{n} \cdot \mu_o \mathbf{H}$ normal to the surface on the free space side, then there must be the same flux density on the conductor side. But this means that there is then a time-varying flux density in the volume of the perfect conductor. Faraday's law, in turn, requires that there be a *curl* of **E** in the conductor. For this to be true, **E** must be finite there, a contradiction of our defini-
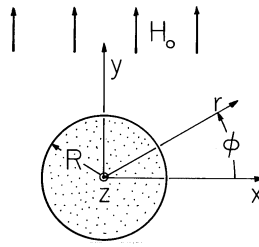
Fig. 8.4.1   Perfectly conducting circular cylinder of radius R in a magnetic field that is y directed and of magnitude H_o far from the cylinder.

tion of the perfect conductor. We conclude that *there can be no normal component of a time-varying magnetic flux density at a perfectly conducting surface.*

$$\boxed{\mathbf{n} \cdot \mu_o \mathbf{H} = 0} \tag{1}$$

Correspondingly, if the $\mathbf{H}$ field is the gradient of the scalar potential Ψ, we find that

$$\frac{\partial \Psi}{\partial n} = 0 \tag{2}$$

on the surface of a perfect conductor. This should be contrasted with the boundary condition for an EQS potential Φ which must be constant on the surface of a perfect conductor. This boundary condition can be used to determine the magnetic field distribution in the neighborhood of a perfect conductor. Once this has been done, Ampère's continuity condition, (1.4.16), can be used to find the surface current density that has been induced by the time-varying magnetic field. With $\mathbf{n}$ directed from the perfect conductor into the region of free space,

$$\boxed{\mathbf{K} = \mathbf{n} \times \mathbf{H}} \tag{3}$$

Because there is no time-varying magnetic field in the conductor, only the tangential field intensity on the free space side of the surface is required in this evaluation of the surface current density.

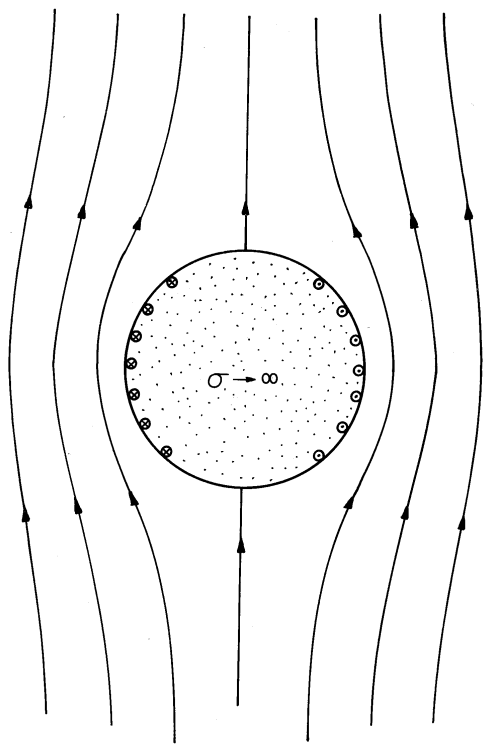**Example 8.4.1.**   Perfectly Conducting Cylinder in a Uniform Magnetic Field

A perfectly conducting cylinder having radius R and extending to $z = \pm\infty$ is immersed in a uniform time-varying magnetic field. This field is y directed and has intensity H_o at infinity, as shown in Fig. 8.4.1. What is the distribution of $\mathbf{H}$ in the neighborhood of the cylinder?

In the free space region around the cylinder, there is no current density. Thus, the field can be written as the gradient of a scalar potential (in two dimensions)

$$\mathbf{H} = -\nabla \Psi \tag{4}$$

The far field has the potential

$$\Psi = -H_o y = -H_o r \sin\phi; \qquad r \to \infty \tag{5}$$

Fig. 8.4.2   Lines of magnetic field intensity for perfectly conducting cylinder in transverse magnetic field.

The condition $\partial\Psi/\partial n = 0$ on the surface of the cylinder suggests that the boundary condition at $r = R$ can be satisfied by adding to (5) a dipole solution proportional to $\sin\phi/r$. By inspection,

$$\Psi = -H_o \sin\phi R\Big(\frac{r}{R} + \frac{R}{r}\Big) \tag{6}$$

has the property $\partial\Psi/\partial r = 0$ at $r = R$. The magnetic field follows from (6) by taking its negative gradient

$$\mathbf{H} = -\nabla\Psi = H_o \sin\phi\,\mathbf{i_r}\Big(1 - \frac{R^2}{r^2}\Big) + H_o \cos\phi\,\mathbf{i_\phi}\Big(1 + \frac{R^2}{r^2}\Big) \tag{7}$$

The current density induced on the surface of the cylinder, and responsible for generating the magnetic field that excludes the field from the interior of the cylinder, is found by evaluating (3) at $r = R$.

$$\mathbf{K} = \mathbf{n} \times \mathbf{H} = \mathbf{i_z} H_\phi(r = R) = \mathbf{i_z} 2H_o \cos\phi \tag{8}$$

The field intensity of (7) and this surface current density are shown in Fig. 8.4.2. Note that the polarity of $\mathbf{K}$ is such that it gives rise to a magnetic dipole field that tends to buck out the imposed field. Comparison of (7) and the field of a two-dimensional dipole, (8.1.21), shows that the induced moment is $id = 2\pi H_o R^2$.
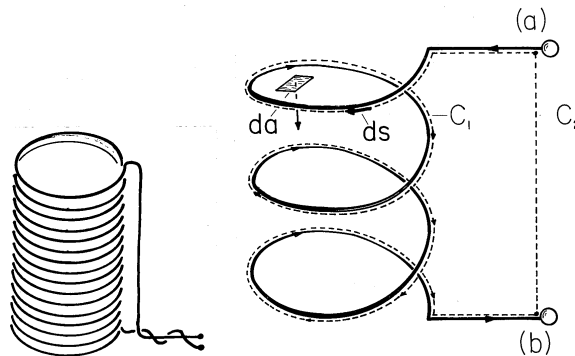
Fig. 8.4.3 A coil having terminals at (a) and (b) links flux through surface enclosed by a contour composed of C_1 adjacent to the perfectly conducting material and C_2 completing the circuit between the terminals. The direction of positive flux is that of $d\mathbf{a}$, defined with respect to $d\mathbf{s}$ by the right-hand rule (Fig. 1.4.1). For the effect of magnetic induction to be negligible in the neighborhood of the terminals, the coil should have many turns, as shown by the inset.

There is an analogy to steady conduction ($\mathbf{H} \leftrightarrow \mathbf{J}$) in the neighborhood of an insulating rod immersed in a conductor carrying a uniform current density. In Demonstration 7.5.2, an electric dipole field also bucked out an imposed uniform field ($\mathbf{J}$) in such a way that there was no normal field on the surface of a cylinder.

Voltage at the Terminals of a Perfectly Conducting Coil. Faraday's law was the underlying reason for the vanishing of the flux density normal to a perfect conductor. By stating this boundary condition in terms of the magnetic field alone, we have been able to formulate the magnetic field of perfect conductors without explicitly solving for the distribution of electric field intensity. It would seem that for the determination of the voltage induced by a time-varying magnetic field at the terminals of the coil, knowledge of the E field would be necessary. In fact, as we now take care to define the circumstances required to make the terminal voltage of a coil a well-defined variable, we shall see that we can put off the detailed determination of $\mathbf{E}$ for Chap. 10.

The EMF at point (a) relative to that at point (b) was defined in Sec. 1.6 as the line integral of $\mathbf{E} \cdot d\mathbf{s}$ from (a) to (b). In Sec. 4.1, where the electric field was irrotational, this integral was then defined as the *voltage* at point (a) relative to (b). We shall continue to use this terminology, which is consistent with that used in circuit theory.

If the voltage is to be a well-defined quantity, independent of the layout of the connecting wires, the terminals of the coil shown in Fig. 8.4.3 must be in a region where the magnetic induction is negligible compared to that in other regions and where, as a result, the electric field is irrotational. To determine the voltage, the integral form of Faraday's law, (1.6.1), is applied to the closed line integral C shown in Fig. 8.4.3.

$$\oint_C \mathbf{E} \cdot d\mathbf{s} = -\frac{d}{dt} \int_S \mu_o \mathbf{H} \cdot d\mathbf{a} \tag{9}$$

The contour goes from the terminal at (a) to that at (b) along the coil wire and closes through a path outside the coil. However, we know that $\mathbf{E}$ is zero along the perfectly conducting wire. Hence, the entire contribution to the line integral comes from the short path between the terminals. Thus, the left side of (9) reduces to

$$\int_{C_1+C_2} \mathbf{E} \cdot d\mathbf{s} = \int_b^a {}_{C_2} \mathbf{E} \cdot d\mathbf{s} = -\int_b^a {}_{C_2} \nabla \Phi \cdot d\mathbf{s}$$
$$= -(\Phi_a - \Phi_b) = -v \tag{10}$$

It follows from Faraday's law, (9), that the terminal voltage is

$$\boxed{v = \frac{d\lambda}{dt}} \tag{11}$$

where λ is the *flux linkage*[3]

$$\boxed{\lambda \equiv \int_S \mu_o \mathbf{H} \cdot d\mathbf{a}} \tag{12}$$

By definition, the surface S spans the closed contour C. Thus, as shown in Fig. 8.4.3, it has as its edge the perfectly conducting coil, C_1, and the contour used to close the circuit in the region where the terminals are located, C_2. If the magnetic induction is negligible in the latter region, the electric field is irrotational. In that case, the specific contour, C_2, is arbitrary, and the EMF between the terminals becomes the voltage of circuit theory.

Our discussion has emphasized the importance of having the terminals in a region where the magnetic induction, $\partial \mu_o \mathbf{H}/\partial t$, is negligible. If a time-varying magnetic field is significant in this region, then different arrangements of the leads connecting the terminals to the voltmeter will result in different voltmeter readings. (We will emphasize this point in Sec. 10.1, where we develop an appreciation for the electric field implied by Faraday's law throughout the free space region surrounding the perfect conductors.) However, there remains the task of identifying configurations in which the flux linkage is not appreciably affected by the layout of leads connected to the terminals. In the absence of magnetizable materials, this is generally realized by making coils with many turns that are connected to the outside world through leads arranged to link a minimum of flux. The inset to Fig. 8.4.3 shows an example. The large number of turns assures a magnetic field within the coil that is much larger than that associated with the wires that connect the coil to the terminals. By intertwining these wires, or at least having them close together, the terminal voltage becomes independent of the detailed wire layout.

Demonstration 8.4.1.   Surface used to Define the Flux Linkage

---

[3] We drop the subscript f on the symbol λ for flux linkage where there is no chance to mistake it for line charge density.
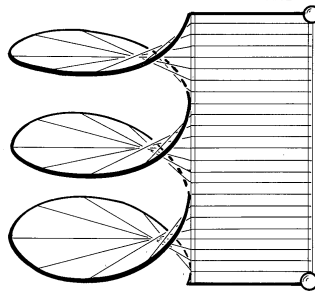
Fig. 8.4.4   To visualize the surface enclosed by the contour $C_1 + C_2$ of Fig. 8.4.3, imagine filling it in with yarn strung on a frame representing the contour.

The surface S used to define λ in (12) is often geometrically complex. It is helpful to picture the surface in terms of a model. Shown in Fig. 8.4.4 is a three-turn coil. The surface is filled in by stringing yarn between a vertical rod joining the terminals in the external region and points on the wire. The surface is filled in by connecting points of decreasing altitude on the rod to points of increasing distance along the wire. Note from Fig. 8.4.3 that $d\mathbf{a}$ and $d\mathbf{s}$ are related by the right-hand rule, where the latter is directed along the contour from the positive terminal to the negative one.

Another way of demonstrating the relationship of the surface to the coil geometry takes advantage of the phenomenon familiar from blowing bubbles. A small coil, closed along the external segment between the terminals, can be dipped into materials like soap solution to form a continuous film having the wire as one continuous edge. In fact, if the film is formed from a material that hardens into a plastic sheet, a permanent model for the surface is obtained.

Inductance.   When the flux linked by the perfectly conducting coil of Fig. 8.4.3 is due entirely to a current i in the coil itself, λ is proportional to i, $\lambda = Li$. Thus, the *inductance* L, defined as

$$L \equiv \frac{\lambda}{i} = \frac{\int_S \mu_o \mathbf{H} \cdot d\mathbf{a}}{i}$$

(13)

becomes a parameter that is only a function of geometric variables and μ_o. In this case, the terminal voltage given by (11) assumes a form familiar from circuit theory.

$$v = L \frac{di}{dt}$$

(14)

The following example illustrates this rule.

Example 8.4.2.   Inductance of a Long Solenoid

In Demonstration 8.2.1, we examined the field of a long N-turn solenoid and found that in the limit where the length d becomes very large, the field intensity along the axis is

$$H_z = \frac{Ni}{d} \tag{15}$$

where i is the current in each turn.

For an infinitely long solenoid this is not only the field on the axis of symmetry but everywhere inside the solenoid. To see this, observe that a uniform magnetic field intensity satisfies both Ampère's law and the flux continuity condition throughout the free space interior region. (A uniform field is irrotational and solenoidal.) Further, with the field given by (15) inside the coil and taken as zero outside, Ampère's continuity condition (1.4.16) is satisfied at the surface of the coil where $K_\phi = Ni/d$. The normal flux continuity condition is automatically satisfied, since there is no flux density normal to the coil surface.

Because the field is uniform over the circular cylindrical cross-section, the magnetic flux $\Phi_\lambda{}^4$ passing through one turn of the solenoid is simply the cross-sectional area A of the solenoid multiplied by the flux density $\mu_o H$.

$$\Phi_\lambda = \mu_o H_z A = \frac{\mu_o A N}{d} i \tag{16}$$

The flux linkage, defined by (12), is obtained by summing the contributions of all the turns.

$$\lambda = \sum_{\text{turns}} \Phi_\lambda = \frac{\mu_o N^2 A}{d} i \tag{17}$$

Thus, from (13),

$$L = \frac{\lambda}{i} = \frac{\mu_o N^2 A}{d} \tag{18}$$

For the circular cylindrical solenoid of radius a, $A = \pi a^2$. The same arguments used to see that the interior field of a solenoid of circular cross-section is given by (15) show that the solenoid can have an arbitrary cross-sectional geometry and the field will still be given by (15) everywhere inside and be zero outside. Thus, (18) is applicable to a solenoid of arbitrary cross-section.

Example 8.4.3.   Dipole Moment Induced in Perfectly Conducting Sphere
by Imposed Uniform Magnetic Field

If a highly conducting material is immersed in a magnetic field, it will modify the field in its vicinity via a surface current that cancels the field in its interior. If the material is spherical, we can superimpose the field of a dipole and the uniform field to exactly satisfy the boundary condition on the conducting surface. For a sphere having radius R in an imposed field $H_o \mathbf{i_z}$, as shown in Fig. 8.4.5, what is the equivalent dipole moment m?

The imposed field is conveniently analyzed into radial and azimuthal components. Then the irrotational and solenoidal field proposed to satisfy the boundary conditions is the sum of that uniform field and the field of a dipole at the origin, as given by (8.3.14) together with the definition (8.3.19).

$$\mathbf{H} = H_o\big(\cos\theta\mathbf{i_r} - \sin\theta\mathbf{i_\theta} \big) + \frac{m}{4\pi}\Big(\frac{2\cos\theta}{r^3}\mathbf{i_r} + \frac{\sin\theta}{r^3}\mathbf{i_\theta} \Big) \tag{19}$$

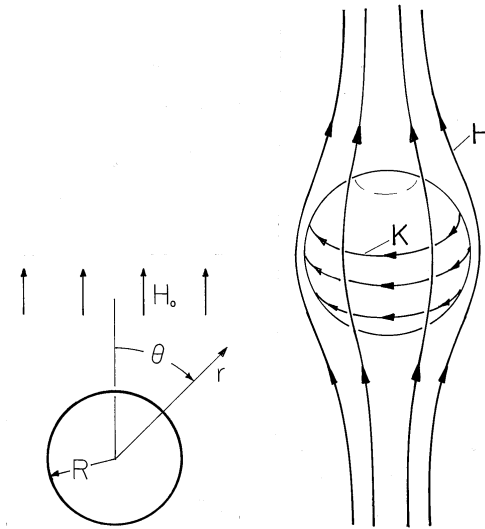[4] We use the symbol Φ_λ for the flux through one turn of a coil or a loop.

Fig. 8.4.5 Immersed in a uniform magnetic field, a perfectly conducting sphere has the same effect as an oppositely directed magnetic dipole.
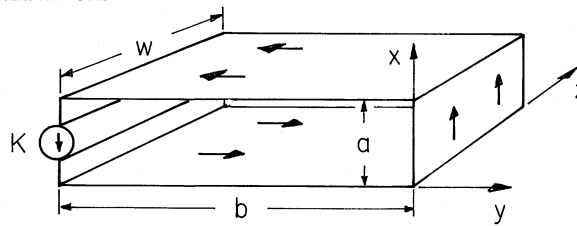

Fig. 8.4.6 One-turn solenoid.

By design, this field already approaches the uniform field at infinity. To satisfy the condition that $\mathbf{n} \cdot \mu_o \mathbf{H} = 0$ at $r = R$,

$$\mu_o H_r(r = R) = 0 \Rightarrow \frac{2m}{4\pi R^3} \cos\theta + H_o \cos\theta = 0 \tag{20}$$

It follows that the equivalent dipole moment is

$$m = -2\pi H_o R^3 \tag{21}$$

The surface currents induced in the sphere which buck out the imposed magnetic flux are responsible for the dipole moment, as illustrated in Fig. 8.4.5.

Example 8.4.4.   One-Turn "Solenoid"

The structure of perfectly conducting sheets shown in Fig. 8.4.6 has width w much greater than a and is excited by a uniform (in the z direction) current per unit length K at $y = -b$.

The H-field solution that satisfies the boundary condition $\mathbf{n} \cdot \mathbf{H} = 0$ and $\mathbf{n} \times \mathbf{H} = \mathbf{K}$ on the perfect conductor is

$$H_z = -K \tag{22}$$

What is the voltage that appears across the current generator? From (11) and (12) we conclude

$$v = \frac{d\lambda}{dt} \tag{23}$$

with

$$\lambda = \int \mu_o \mathbf{H} \cdot d\mathbf{a} = \mu_o K a b = \mu_o \frac{ab}{w} i$$

where i is the total current supplied by the generator. The voltage is thus

$$v = L\frac{di}{dt} \tag{24}$$

where

$$L = \mu_o \frac{ab}{w}$$

8.5 PIECE-WISE MAGNETIC FIELDS

In a typical physical situation to which the scalar potential is applicable, layers of wire are used to make a winding that is thin compared to other dimensions of interest. Currents are then confined to surfaces that separate the regions where $\mathbf{H}$ is irrotational. Thus, the sources of the magnetic field intensity can be represented as surface currents. The field produced by these currents is then found by choosing source-free solutions in the space surrounding the current-carrying surfaces and "connecting" these solutions across the surfaces by the proper boundary conditions. This procedure is analogous to finding EQS potentials produced by charge sheets in Chap. 5. Solutions to Laplace's equation were set up on the two sides of a charge sheet and the jump in normal $\epsilon_o\mathbf{E}$ adjusted to equal the surface charge density.

In the MQS situation, the H field obeys Ampère's continuity condition, (1.4.16).

$$\mathbf{n} \times (\mathbf{H}^a - \mathbf{H}^b) = \mathbf{K} \tag{1}$$

At this same surface, the magnetic flux continuity condition, (1.7.6), also applies.

$$\mathbf{n} \cdot (\mu_o\mathbf{H}^a - \mu_o\mathbf{H}^b) = 0 \tag{2}$$

Remember that in Chap. 5, continuity of tangential $\mathbf{E}$ was implied by making the electric potential continuous. By contrast, according to (1), where there is a surface current density, the tangential $\mathbf{H}$ is discontinuous and this implies that *the magnetic scalar potential Ψ is not generally continuous.* To see this, consider the application of Ampère's integral law to an incremental surface that is pierced by the surface current density, as shown in Fig. 8.5.1. If $\mathbf{H}$ is finite, then in the limit where the width w goes to zero, the contributions to the line integral from the segments $B \rightarrow B'$ and $A' \rightarrow A$ vanish, and so

$$\oint_C \mathbf{H} \cdot d\mathbf{s} = \int_S \mathbf{J} \cdot d\mathbf{a} \Rightarrow -(\nabla\Psi^a - \nabla\Psi^b) \cdot \mathbf{i}_s = \mathbf{K} \cdot \mathbf{i}_n \tag{3}$$
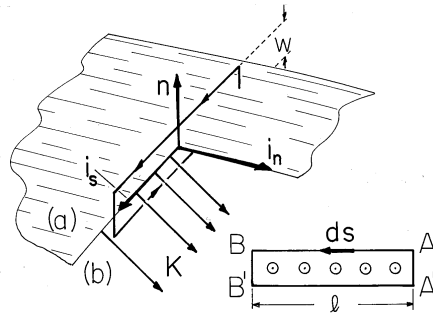
Fig. 8.5.1   Contour enclosing surface current density **K** on surface having normal **n**. Integration of Ampère's law on surface enclosed by the contour shows that the magnetic scalar potential is, in general, discontinuous across the surface.

where the unit vectors $\mathbf{i}_s$ and $\mathbf{i}_n$ are defined in Fig. 8.5.1.

Multiplication of (3) by the incremental line element ds and integration over the length of the incremental surface gives

$$-\int_A^B \left(\nabla\Psi^a - \nabla\Psi^b\right)\cdot\mathbf{i}_s ds = \int_A^B \mathbf{K}\cdot\mathbf{i}_n ds \tag{4}$$

In view of the gradient integral theorem, (4.1.16), the integrals on the left can be carried out to obtain

$$(\Psi_B - \Psi_A) - (\Psi_{B'} - \Psi_{A'}) = -\int_A^B \mathbf{K}\cdot\mathbf{i}_n ds \tag{5}$$

Now think of $A-A'$ as a fixed reference position on the surface, where Ψ_A is defined as being equal to $\Psi_{A'}$. It then follows that the discontinuity in Ψ at the location $B-B'$ is a measure of the net current passing normal to the strip joining $A-A'$ to $B-B'$.

A further contrast with the electric field comes from the normal field continuity condition, (2). *At a surface carrying a surface current density in free space, the normal derivative of Ψ is continuous.*

The following example shows how to find Ψ, and hence **H**, when a surface current distribution is given.

Example 8.5.1.   The Spherical Coil

The magnetic field intensity produced inside a properly wound spherical coil has the important property that it is uniform. This should be contrasted with the field of a long solenoid that is uniform only to the extent that the fringing field can be neglected.

The coil is wound of thin wire so that the turns density is sinusoidally distributed between the north and south poles of a sphere. To the extent that we can disregard the slight pitch in the coil needed to connect the loops with each other, loops of appropriately varying diameter, spaced evenly as projected onto the z axis,
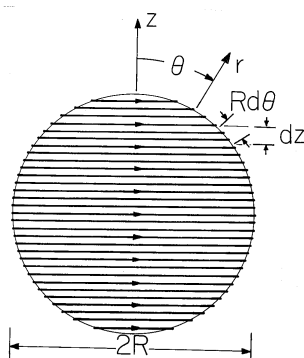
Fig. 8.5.2   Cross-section of "flux ball" consisting of sphere with winding on its surface that is of uniform turns density with respect to the z axis.

automatically simulate such a distribution. The coil, with a radius R and a wire carrying the current i, is shown in Fig. 8.5.2.

To deduce the surface current density representing this winding, note that the density of turns on the surface is the total number, N, divided by the total length, $2R$, and so the number of turns in the incremental length dz is $(N/2R)dz$. Because $z = r\cos\theta$, a differential length dz corresponds to an angular increment $d\theta$: $dz = -\sin\theta R d\theta$. Therefore, the number of turns in the differential length $R d\theta$ as measured along the periphery of the sphere is $(N/2R)\sin\theta$. With each turn carrying the current i, the surface current density is

$$\mathbf{K} = \mathbf{i}_\phi \frac{N}{2R} i \sin\theta \tag{6}$$

In the spaces interior and exterior to the surface of the sphere, $\mathbf{H}$ is both irrotational and solenoidal. Hence, it is represented by scalar magnetic potentials.

The ϕ component of (1) is the link between the surface current density and the induced field.

$$H_\theta^a - H_\theta^b = \frac{N}{2R} i \sin\theta \tag{7}$$

To obtain H_θ, the derivative of Ψ with respect to θ must be taken, and this suggests that the θ dependence of Ψ be taken as $\cos\theta$. The field is finite at the origin and zero at infinity, so, from the three solutions to Laplace's equation given in Sec. 5.9, we select

$$\Psi = C(r/R)\cos\theta; \qquad r < R \tag{8}$$

$$\Psi = A(R/r)^2 \cos\theta; \qquad r > R \tag{9}$$

The continuity conditions, used now to determine the coefficients A and C, are in terms of the field intensity. Thus, (8) and (9) are used to write $\mathbf{H}$ in the two regions as

$$\mathbf{H} = -\frac{C}{R}(\mathbf{i_r}\cos\theta - \mathbf{i}_\theta \sin\theta); \qquad r < R \tag{10}$$

$$\mathbf{H} = \frac{A}{R}(R/r)^3(\mathbf{i_r}2\cos\theta + \mathbf{i}_\theta \sin\theta); \qquad r > R \tag{11}$$

Substitution of the appropriate components into the continuity conditions, (2) and (7), gives

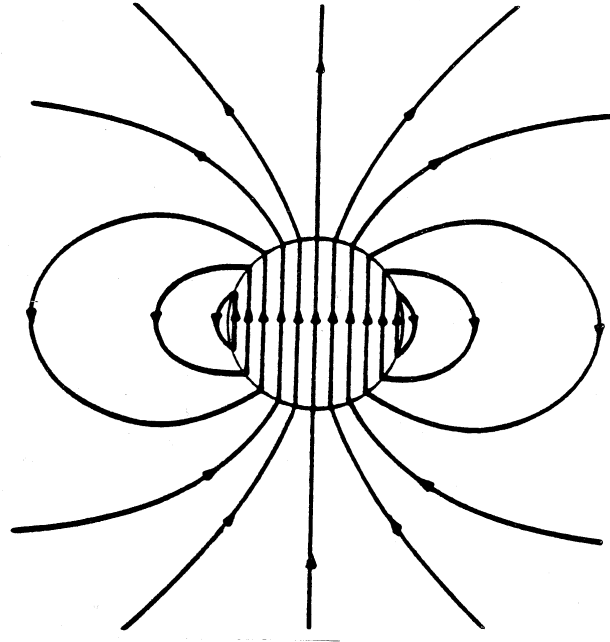$$-\frac{C}{R} = \frac{2A}{R} \tag{12}$$

Fig. 8.5.3   Magnetic field intensity of "flux-ball" shown in Fig. 8.5.2.

$$\frac{A}{R} - \frac{C}{R} = \frac{Ni}{2R} \tag{13}$$

Thus, the magnetic field intensity of (10) and (11) is evaluated by setting $C = -2A = -Ni/3$.

$$\mathbf{H} = \frac{Ni}{3R}(\mathbf{i_r}\cos\theta - \mathbf{i}_\theta\sin\theta); \qquad r < R \tag{14}$$

$$\mathbf{H} = \frac{Ni}{6R}(R/r)^3(\mathbf{i_r}2\cos\theta + \mathbf{i}_\theta\sin\theta); \qquad r > R \tag{15}$$

The exterior lines of magnetic field intensity are those of a dipole, while the interior field is uniform. Thus, the total picture, shown in Fig. 8.5.3, is one of field lines circulating from south to north inside the sphere and back from north to south on the outside around currents that follow lines of equilatitude around the sphere.

The magnetic potential follows by substituting $C = -2A = -Ni/3$ for C and A in (8) and (9).

$$\Psi = -\frac{Ni}{3}\frac{r}{R}\cos\theta; \qquad r < R \tag{16}$$

$$\Psi = \frac{Ni}{6}(R/r)^2\cos\theta; \qquad r > R \tag{17}$$

Note that these potentials are equal at the equator of the sphere and become increasingly disparate as the poles are approached. With the vertical dimension used to denote Ψ, a sketch of Ψ evaluated in a plane of fixed ϕ would appear as shown in Fig. 8.5.4. Inside, Ψ slopes linearly from its highest value at the south pole to its lowest at the north. Outside, Ψ has its highest value at the north pole and lowest at
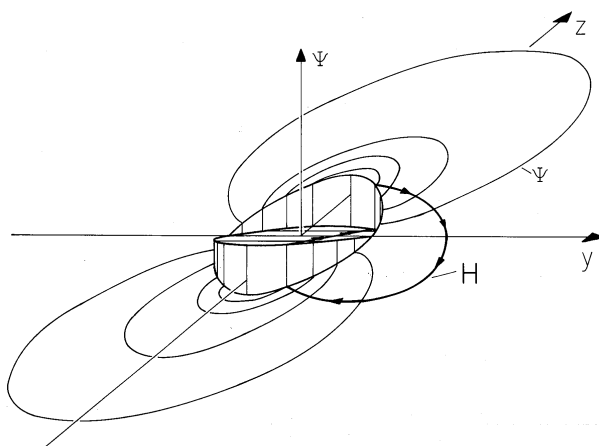
Fig. 8.5.4 Magnetic scalar potential for "flux ball" of Fig. 8.5.2. The vertical axis is Ψ. A line of **H** closes on itself as it circulates around surface current, going down the potential "hills" inside and outside the sphere and recovering its altitude at the surfaces of discontinuity at $r = R$, containing the surface current density.

the south. This is consistent with the picture afforded by Fig. 8.5.1 and (5). Even though it closes on itself, the line of **H** shown goes continuously "down hill." The potential Ψ regains its altitude in the region of discontinuity.

Finally, we illustrate the computation of the inductance of a coil modeled by a surface current and represented in terms of the magnetic scalar potential. To compute the total flux linked by the winding, first consider the flux linked by one turn at the location $r = R$ and $\theta = \theta'$. Using the flat surface at $z' = R\cos\theta'$ that is enclosed by this circular turn, the flux is

$$\Phi_\lambda = \int_0^{R\sin\theta'} \mu_o H_z 2\pi r dr = \pi(R\sin\theta')^2 \mu_o H_z \tag{18}$$

In this particular problem, H_z is uniform inside the sphere, so this integration amounts to multiplying the area enclosed by the turn by the normal flux density.

The turns density multiplied by $Rd\theta$ gives the number of turns linking this flux in an increment of peripheral length. Thus, the total flux is obtained by carrying out a second integration over all of the turns.

$$\lambda = \int_0^\pi \Phi_\lambda \frac{N}{2R} \sin\theta' R d\theta' = \int_0^\pi i\frac{\pi N^2 R\mu_o}{6} \sin^3\theta' d\theta' = Li \tag{19}$$

$$L \equiv \frac{2}{9}\pi N^2 \mu_o R \tag{20}$$

Demonstration 8.5.1.   Field and Inductance of a Spherical Coil

In the experiment shown in Fig. 8.5.5, the "flux ball" has 64 turns and a radius of $R = 5$ cm. The turns are wound on a plastic sphere that essentially has the magnetic properties of free space.
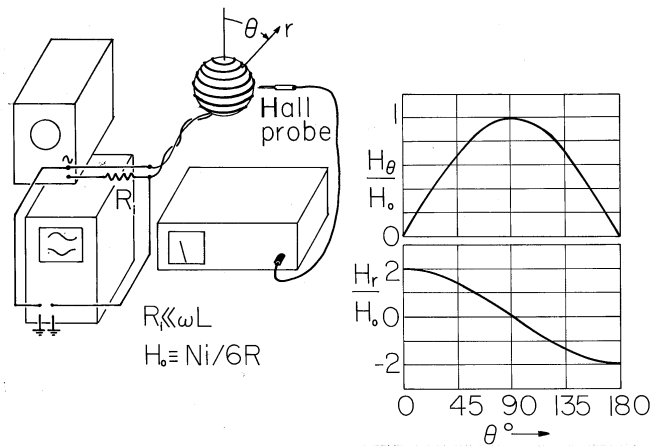
Fig. 8.5.5   Demonstration of fields surrounding the magnetic "flux ball."

The Hall magnetometer makes it possible to probe the magnitude and direction of the field outside the coil. For example, at the north pole, where the magnetic flux density is perpendicular to the sphere surface, the flux density is vertical and for $i = 1$ A predicted by either (14) or (15) to be $\mu_o Ni/3R = 5.36 \times 10^{-4}T = 5.36$ gauss. The inductance is determined by measuring the voltage and current, varying the frequency to determine that it is high enough to assure that the resistance of the coil plays a negligible role in the terminal impedance (the impedance should be of magnitude ωL, and hence vary linearly with frequency). The inductance predicted by (20) is 180 μH, and the value measured using the oscilloscope is typically within 10 percent.

8.6 VECTOR POTENTIAL AND THE BOUNDARY VALUE POINT OF VIEW

We have found that many interesting MQS cases can be treated by the use of the scalar potential obeying Laplace's equation. The vector potential, defined by (8.1.1), is necessary when analyzing fields with nonzero curl. There are other cases as well in which its use may be advantageous. The vector potential is the natural variable for evaluating the flux passing through a surface. In view of (8.1.1), integration of the flux density over the open surface S of Fig. 8.6.1 gives
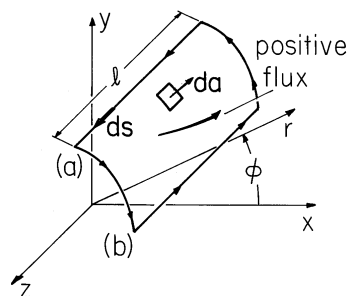
$$\lambda = \int_S \mu_o \mathbf{H} \cdot d\mathbf{a} = \int_S \nabla \times \mathbf{A} \cdot d\mathbf{a} \tag{1}$$

and it follows from Stokes' theorem that this flux is equal to the line integral of $\mathbf{A} \cdot d\mathbf{s}$ around the contour enclosing the surface.

$$\boxed{\lambda = \oint_C \mathbf{A} \cdot d\mathbf{s}} \tag{2}$$
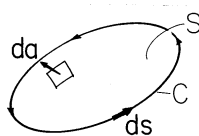
Fig. 8.6.1 Open surface S having area element $d\mathbf{a}$ enclosed by contour C having directed differential length $d\mathbf{s}$.

Fig. 8.6.2 Surface S with sides of length l parallel to the z axis at locations (a) and (b). The contour direction is consistent with the flux being positive, as shown.

In certain important cases, $\mathbf{A}$ has only one component and a vector field is again represented in terms of one scalar function. Two such cases are identified in the following subsections.

Vector Potential for Two-Dimensional Fields. Suppose that the flux density is parallel to the $x-y$ plane and is independent of z. It can then be represented by a vector potential having only a z component.

$$\mathbf{A} = A_z(x,y)\mathbf{i_z} \tag{3}$$

Note that the divergence of this $\mathbf{A}$ is automatically zero and that in Cartesian coordinates, the components of the flux density are given in terms of A_z by

$$\mu_o\mathbf{H} = \nabla \times \mathbf{A} = \frac{\partial A_z}{\partial y}\mathbf{i_x} - \frac{\partial A_z}{\partial x}\mathbf{i_y} \tag{4}$$

Consider now the evaluation of the net flux of magnetic flux density through a surface S that has length l in the z direction, as shown in Fig. 8.6.2. The points (a) and (b) denote the coordinates of the corners of the contour enclosing S. The contour consists of a pair of parallel straight segments of length l parallel to the z axis, one at the location (a) in the $x-y$ plane and the other at (b), and contours joining (a) and (b) in $x-y$ planes. Contributions to the contour integral, (2), from these latter segments of C are zero, because $\mathbf{A}$ is perpendicular to $d\mathbf{s}$. Integration along the z-directed segments amounts to multiplication of A_z evaluated at (a) or (b) by the length of the segment. Thus, (1) becomes

$$\boxed{\lambda = l(A_z^a - A_z^b)} \tag{5}$$
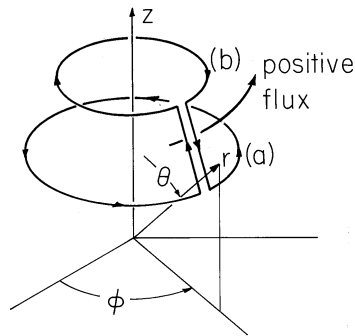
Fig. 8.6.3   Difference between axisymmetric stream function Λ_s evaluated at (a) and (b) is net flux through surface enclosed by the contour shown.

The vector potential at (a) relative to (b) is the net magnetic flux per unit length passing through a surface of unit length in the z direction subtended between the two points and a corresponding pair at unity distance along the z axis. Note that the flux has a sign, relative to the direction of the contour integration, governed by the right-hand rule (Fig. 1.4.1).

Vector Potential for Axisymmetric Fields in Spherical Coordinates.
If the magnetic flux density is invariant with respect to rotation around the z axis, having components in the r and θ directions only, the vector potential again has a single component.

$$\mathbf{A} = A_\phi(r, \theta)\mathbf{i}_\phi \tag{6}$$

The net flux through the annular surface "spanned" over the contour shown in Fig. 8.6.3, having constant outer and inner radii denoted by (a) and (b), respectively, is given by the contributions to (2) of the azimuthal segments, A_ϕ multiplied by the circumferences. The contour is closed by adjacent oppositely directed segments joining points (a) and (b) in a plane of constant ϕ. Thus, the contributions to the line integral of (2) from these segments cancel, even if $\mathbf{A}$ had components in the direction of $d\mathbf{s}$ on these segments. Thus, the net flux through the annulus is simply the *axisymmetric stream function* Λ at (a) relative to that at (b).[5]
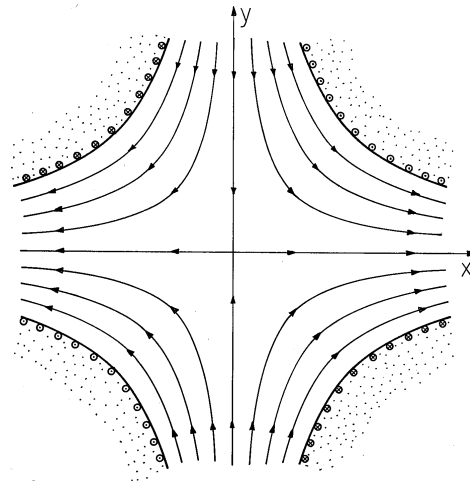
$$\boxed{\lambda = \Lambda_s^a - \Lambda_s^b} \tag{7}$$

where

$$\Lambda_s \equiv 2\pi r \sin \theta A_\phi \tag{8}$$

Lines of flux density are tangential to the axisymmetric surfaces of constant Λ_s. Just as A_z provides a ready visualization of the flux lines in two dimensions, Λ_s portrays the axisymmetric flux lines.

---

[5] With $\mathbf{A}$ used to represent the velocity distribution of an incompressible fluid, Λ_s (or $\Lambda_s/2\pi$) is called Stokes' stream function.

Fig. 8.6.4 Surfaces of constant A_z and hence lines of magnetic field intensity for field trapped between perfectly conducting electrodes.

Boundary Value Solution by "Inspection".   In two-dimensional configurations, any surface of constant A_z can be replaced by the surface of a perfect conductor. Moreover, in the free space region between conductors, A_z satisfies Laplace's equation. Thus, any two-dimensional configuration from Chaps. 4 and 5 can be replaced by one where the potential lines are field lines. The equipotential (constant Φ) surfaces of the EQS perfect conductors become the perfectly conducting (constant A_z) surfaces of an MQS system.

Illustration.   Field Trapped between Hyperbolic Perfect Conductors

The two-dimensional potential distribution of Example 4.1.1 suggests the vector potential $A_z = \Lambda_o xy/a^2$. The lines of magnetic field intensity, which are the surfaces of constant A_z, are shown in Fig. 8.6.4. Here, the surfaces $A_z = \pm\Lambda_o$ are taken as being the surfaces of perfect conductors. Thus, the current density on the surfaces of these conductors are, given by using (4) to determine **H** and, in turn, (8.4.3) to find K_z. These currents shield the fields from the volume of the perfect conductors. The net flux per unit length passing downward between the upper pair of conductors is [in view of (7)] simply $2\Lambda_o$.

This solution is the superposition of the fields of four line currents. Two directed in the $+z$ direction are at infinity in the first and third quadrants, while two in the $-z$ direction are in the second and fourth quadrants.

Example 8.6.1.   Field and Inductance of Oppositely Directed Currents
in Parallel Perfectly Conducting Cylinders

The cross-section of a pair of parallel perfectly conducting cylinders that extend to $\pm\infty$ in the z direction is shown in Fig. 8.6.5. The conductors have the same geometry as in the EQS case considered in Example 4.6.3. However, they should be regarded as shorted at one end and driven by a current source i at the other. Thus, current in the $+z$ direction in the right conductor is returned in the left conductor.
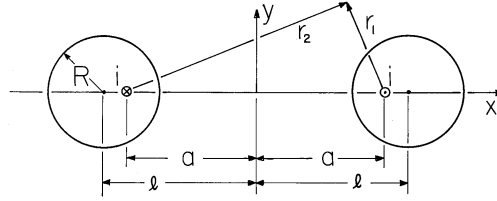
Fig. 8.6.5 Cross-section of perfectly conducting parallel conductors having radius R and spacing $2l$. Fields of oppositely directed line currents having spacing $2a$ are shown to satisfy normal flux boundary condition on circular cylindrical surfaces of conductors.

Although the net current in each conductor is given, its distribution on the surface of the conductors is to be determined.

Example 4.6.3 suggests our strategy. Instead of superimposing the potentials Φ of a pair of line charges of opposite sign, we superimpose the A_z of oppositely directed line currents. With r_1 and r_2 the distances from the observer coordinate to the source coordinates, defined in Fig. 8.6.5, it follows from the vector potential for a line current given by (8.1.16) that

$$A_z = -\frac{\mu_o i}{2\pi}(ln\, r_1 - ln\, r_2) \tag{9}$$

With the identification of variables

$$A_z \to \Phi; \qquad \frac{\mu_o i}{2\pi} \to \frac{\lambda_l}{2\pi\epsilon_o} \tag{10}$$

this expression is identical to that for the antidual EQS configuration, (4.6.18). We can conclude that the line currents should be located at $a = (l^2 - R^2)^{1/2}$, and that the constant k used in that deduction (4.6.20) is identified using (10).

$$k \equiv \exp\left(\frac{2\pi\Lambda}{\mu_o i}\right) = \frac{l+a}{R} \tag{11}$$

Here, the potential U in (4.6.20) is replaced by the flux per unit length Λ. Thus, the surfaces of constant A_z are circular cylinders and represent the field lines shown in Fig. 8.6.6.

The inductance per unit length L is now deduced from (11).

$$L \equiv \frac{2\Lambda}{i} = \frac{\mu_o}{\pi}ln\left(\frac{l+a}{R}\right) = \frac{\mu_o}{\pi}ln\left|\frac{l}{R} + \sqrt{\left(\frac{l}{R}\right)^2 - 1}\right| \tag{12}$$

In the limit where the conductors represent wires that are thin compared to their spacing, the inductance per unit length of (12) is approximated using (4.6.28).

$$L \approx \frac{\mu_o}{\pi}ln\left(\frac{2l}{R}\right) \tag{13}$$

Once the vector potential has been determined, it is possible to evaluate the distribution of current density on the conductors. Note that the currents tend to concentrate on the inside surfaces of the conductors, where the magnetic field intensity is more intense.
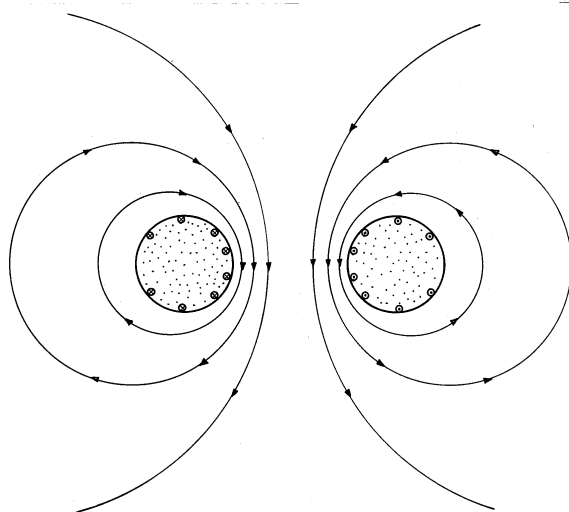
Fig. 8.6.6   Surfaces of constant A_z and hence lines of magnetic field intensity for the parallel conductor configuration shown in the same cross-sectional view by Fig. 8.6.5.

We are one step short of a general relationship between the capacitance per unit length and inductance per unit length of a pair of parallel perfect conductors, regardless of the cross-sectional geometry. With Φ and A_z defined as zero on one of the conductors, evaluated on the other conductor they represent the voltage and the flux linkage per unit length, respectively. Thus, with the understanding that Φ and A_z are evaluated on the second conductor, $L = A_z/i$, and $C = \lambda_l/\Phi$, (4.6.5). Here, i and λ_l, respectively, are the line current and line charge density that give rise to the same fields as do those sources actually on the surfaces of the conductors. These quantities are related by (10), so we can conclude that regardless of the cross-sectional geometry, the product of the inductance per unit length and the capacitance per unit length is

$$LC = \frac{A_z \lambda_l}{i\Phi} = \mu_o \epsilon_o = \frac{1}{c^2} \tag{14}$$

where c is the velocity of light (3.1.16).

Note that inductance per unit length of parallel circular conductors given by (12) and the capacitance per unit length for the same conductors under "open circuit" conditions (4.6.27) satisfy the general relation (14).

Method of Images.   In the presence of a planar perfect conductor, the zero normal flux condition can be satisfied by symmetrically mounting source distributions on both sides of the plane. This approach is familiar from Sec. 4.7, where the boundary condition required a plane of symmetry on which the tangential electric field was zero. Here we require that the field intensity be tangential to the boundary. For two-dimensional configurations, the analogy between the electric potential and A_z makes the image method of Sec. 4.7 directly applicable here. In both cases, the symmetry plane is one of constant potential (Φ or A_z).
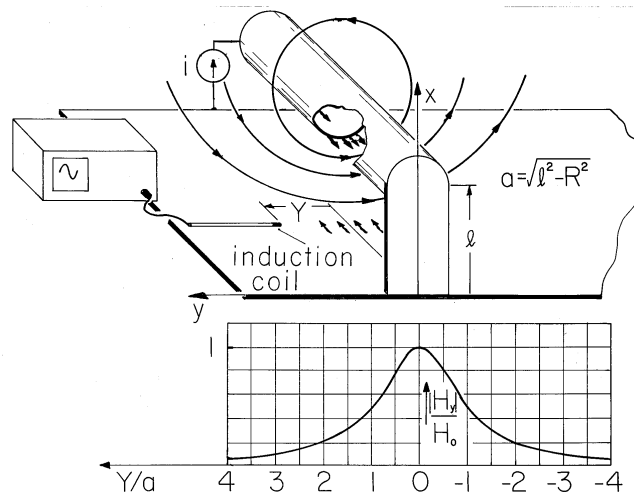
Fig. 8.6.7   With the frequency high enough so that the currents distribute themselves with a negligible normal flux density on the conductors, the field intensity tangential to the conducting plane is that predicted by (16) and shown by the graph. At low frequencies, the current tends to be uniformly distributed in the planar conductor.

The most obvious example is an infinitely long line current at a distance $d/2$ from a perfectly conducting plane. If Fig. 4.7.1 were a picture of line charges rather than point charges, this would be the dual situation. The appropriate image is then an oppositely directed line current located at a distance $d/2$ to the other side of the perfectly conducting plane. By making a pair of symmetrically located line currents the image for this pair of currents, the boundary condition on yet another plane can be satisfied, the analog to the configuration of Fig. 4.7.3.

The following demonstration is intended to emphasize that the perfectly conducting symmetry plane carries a surface current that terminates the field in the region of interest.

Demonstration 8.6.1.   Surface Currents Induced in Ground Plane by Overhead Conductor

The metal cylinder mounted over a metal ground plane shown in Fig. 8.6.7 is familiar from Demonstration 4.7.1. Rather than being insulated from the ground plane and driven by a voltage source, this cylinder is shorted to the ground plane at one end and driven by a current source at the other. The height l is small compared to the length, so that the two-dimensional model describes the field distribution in the midregion.

A probe is used to measure the magnetic flux density tangential to the metal ground plane. The distribution of this field, and hence of the surface current density in the adjacent metal, can be determined by recognizing that the ground plane boundary condition of no normal flux density is met by symmetrically mounting a distribution of oppositely directed currents below the metal sheet. This is just what was done in determining the fields for the pair of cylindrical conductors, Fig. 8.6.5.

Thus, (9) is the image solution for the region $x \geq 0$. In terms of x and y,

$$A_z = -\frac{\mu_o i}{2\pi} ln \frac{\sqrt{(a-x)^2 + y^2}}{\sqrt{(a+x)^2 + y^2}} \tag{15}$$

The flux density tangential to the ground plane at the location $y = Y$ is

$$\mu_o H_y(x = 0) = -\frac{\partial A_z}{\partial x}(x = 0) = -\mu_o \frac{i}{\pi a}\left[\frac{1}{1 + \left(\frac{Y}{a}\right)^2}\right] \tag{16}$$

Normalized to $H_o = i/\pi a$, this distribution is shown as a function of the probe position, Y, in the inset to Fig. 8.6.7.

The role of the surface current density implied by this tangential field is demonstrated by the same probe measurement of the magnetic flux density normal to the conducting sheet. Provided that the frequency is high enough so that the sheet does indeed behave as a perfect conductor, this flux density is small compared to that tangential to the sheet. This is also true at the surface of the cylindrical conductor.

To appreciate the physical origins of this distribution, a dc current source is used in place of the ac source. The distribution of current in the sheet is then dictated by the rules of steady conduction, as enunciated in the first half of Chap. 7. If the sheet is long enough compared to its width, the current is uniformly distributed over the sheet and over the cross-section of the cylinder. By contrast with the high-frequency ac case, where the field is terminated by surface currents in the sheet, the magnetic field now extends below the sheet.

The method of images is not restricted to the two-dimensional situations where there is a convenient analogy between Φ and A_z. In the following example, involving a three-dimensional field, the symmetry conditions are viewed without the aid of the vector potential.

Example 8.6.2.   Current Loop above a Perfectly Conducting Plane

A current loop with time-varying current i is mounted a distance h above a perfectly conducting plane, as shown in Fig. 8.6.8. Its axis is inclined at an angle θ with respect to the normal to the plane. What is the net field produced by the current loop and the currents it induces in the plane?

To satisfy the boundary condition in the plane of the perfectly conducting sheet, an image loop is mounted as shown in Fig. 8.6.9. For each current segment in the actual loop, there is a segment in the image loop giving rise to an oppositely directed vertical component of **H**. Thus, the net normal flux density in the plane of the perfect conductor is zero.

Two-Dimensional Boundary Value Problems.   The vector potential of a two-dimensional field parallel to the $x - y$ plane is z directed and thus only one scalar function describes fully the associated field, as already pointed out earlier. In problems in which currents are confined to the boundaries, the scalar potential can be used as effectively as the vector potential. The lines of steepest descent of the scalar potential are the lines of constant height of the vector potential. When the
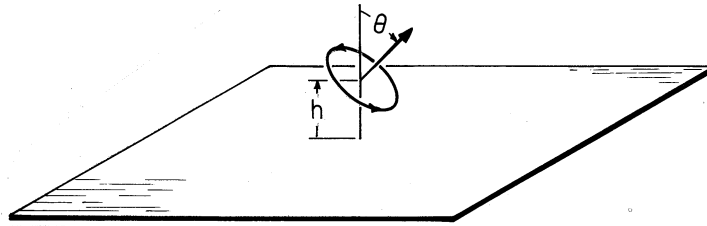
Fig. 8.6.8 Current loop at distance h above a perfectly conducting plane.
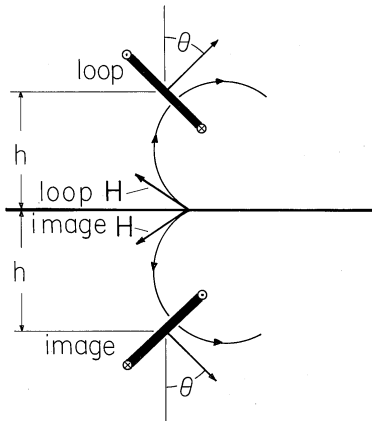

Fig.   **8.6.9** Cross-section
of configuration of Fig. 8.6.8, showing image dipole giving rise to field
that cancels the flux density normal to the planar perfect conductor.

region of interest contains current distributions, then use of the vector potential is
required. We shall consider both situations in the examples to follow.

Example 8.6.3.   Inductive Attenuator

The cross-section of two conducting electrodes that extend to infinity in the $\pm z$
directions is shown in Fig. 8.6.10. The time-varying current in the $+z$ direction
in the electrode at $y = b$ is returned in the $-z$ direction through the ⊔-shaped
electrode. This current is so rapidly varying that the electrodes behave as though
they were perfectly conducting. The gaps of width Δ insulating the electrodes from
each other are small compared to the other dimensions of interest. The magnetic
flux (per unit length in the z direction) passing through these gaps in the directions
shown is defined as $\Lambda(t)$.

The magnetic fields are two dimensional and there are no sources in the region
of interest. Thus, $\mu_o\mathbf{H}$ can be represented in terms of A_z, which satisfies

$$\nabla^2 A_z = 0 \tag{17}$$

The walls are perfectly conducting in the sense that they are modeled as having no
normal $\mu_o\mathbf{H}$. This means that A_z is constant on these walls. We define A_z to be
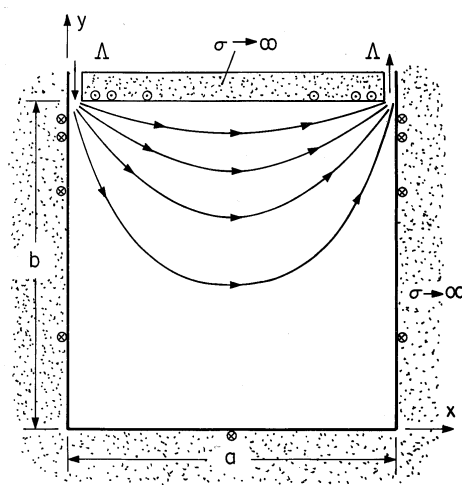zero on the vertical and bottom walls. Thus, A_z must be equal to Λ on the upper

Fig. 8.6.10   Cross-section of inductive attenuator.

electrode, so that the flux per unit length in the z direction through the gaps is Λ.

$$A_z(0,y) = 0, \quad A_z(a,y) = 0, \quad A_z(x,0) = 0, \quad A_z(x,b) = \Lambda \tag{18}$$

The boundary value problem is now formally identical to the EQS capacitive attenuator that was the theme of Sec. 5.5, with the identification of variables

$$\Phi \to A_z, \qquad V \to \Lambda \tag{19}$$

Thus, it follows from (5.5.9) that

$$A_z = \sum_{\substack{n=1 \\ \text{odd}}}^{\infty} \frac{4\Lambda(t)}{n\pi} \frac{\sinh\left(\frac{n\pi}{a}y\right)}{\sinh\left(\frac{n\pi b}{a}\right)} \sin\left(\frac{n\pi}{a}x\right) \tag{20}$$

The lines of magnetic flux density are the lines of constant A_z. They are the *equipotential* "lines" of Fig. 5.5.3, shown in Fig. 8.6.10 with arrows added to indicate the field direction. Remember, there is a z-directed surface current density that is proportional to the tangential field intensity. For the flux lines shown, K_z is out of the page in the upper electrode and returned into the page on the side walls and (to an extent determined by b relative to a) on the bottom wall as well.

From the cross-sectional view given by Fig. 8.6.10, the provision for the current through the driven plate at the top to recirculate through the side and bottom plates is not shown. The following demonstration emphasizes the implied current paths at the ends of the configuration.

Demonstration 8.6.2.   Inductive Attenuator

One configuration described by Example 8.6.3 is shown in Fig. 8.6.11. Here the upper plate is shorted to the adjacent walls at the near end and driven at the far end through a step-down transformer by a 20 kHz oscillator. The driving voltage $v(t)$ at the far end of the upper plate is measured by means of an oscilloscope. The lower

plate is shorted to the side walls at the far end and also connected to these walls at the near end, but in such a way that the induced current $i(t)$ can be measured by means of a current probe.

The walls and upper and lower plates are made from brass or copper. To insure that the resistances of the plate terminations are negligible, they are made from heavy copper wire with the connections soldered. (To make it possible to adjust the spacing b, braided wire is used for the shorts on the lower electrode.)

If the length w of the plates in the z direction is large compared to a and b, **H** within the volume follows from (20). The surface current density K_z in the lower plate then follows from evaluation of the tangential **H** on its surface. In turn, the total current follows from integration of K_z over the width, a, of the plate.

$$i = -\frac{1}{\mu_o} \sum_{\substack{n=1 \\ \text{odd}}}^{\infty} \frac{16\Lambda}{2n\pi} \frac{1}{\sinh\left(\frac{n\pi b}{a}\right)} \tag{21}$$

With the objective of relating this current to the driving voltage, note that (8.4.11) gives

$$v = w\frac{d\Lambda}{dt} \tag{22}$$

so that with the driving voltage a sinusoid of magnitude V,

$$v = V\cos(\omega t) \Rightarrow \Lambda = \frac{V}{w\omega}\sin(\omega t) \tag{23}$$

Thus, in terms of the driving voltage, the output current is $i_o \sin(\omega t)$, where it follows from (21) and (23) that

$$i_o = -I \sum_{\substack{n=1 \\ \text{odd}}}^{\infty} \frac{1}{2n\sinh\left(\frac{n\pi b}{a}\right)}; \qquad I \equiv \frac{16V}{\pi w\omega\mu_o} \tag{24}$$

We have found that the output current, normalized to I, has the dependence on spacing between upper and lower plates shown by the inset to Fig. 8.6.11. With the spacing b small compared to a, almost all of the current through the upper plate is returned in the lower one, and the field between is essentially uniform. As the spacing b becomes comparable to the distance a between the side walls, most of the current through the upper electrode is returned in these side walls. Thus, for large b/a, the normalized output current of Fig. 8.6.11 reflects the exponential decay in the $-y$ direction of the field.

Value is added to this demonstration if it is compared to its EQS antidual, Demonstration 5.5.1. For the EQS configuration, the lower plate was properly constrained to essentially the same potential as the walls by connecting it to these side walls through a resistance (which was then used to measure the induced current). Up to frequencies above 100 Hz in the EQS case, this resistance could be as high as that of the oscilloscope (say 1 MΩ) and still constrain the lower plate to essentially the same zero potential as the walls. In the MQS case, we did not use a resistance to connect the lower plate to the side walls (and hence provide a means of measuring the output current), because that resistance would have had to be extremely low, even at 20 kHz, to prevent flux from leaking through the gaps between the lower plate and the side walls. We used the current probe instead. The effects of finite conductivity in MQS systems are the subject of Chap. 10.
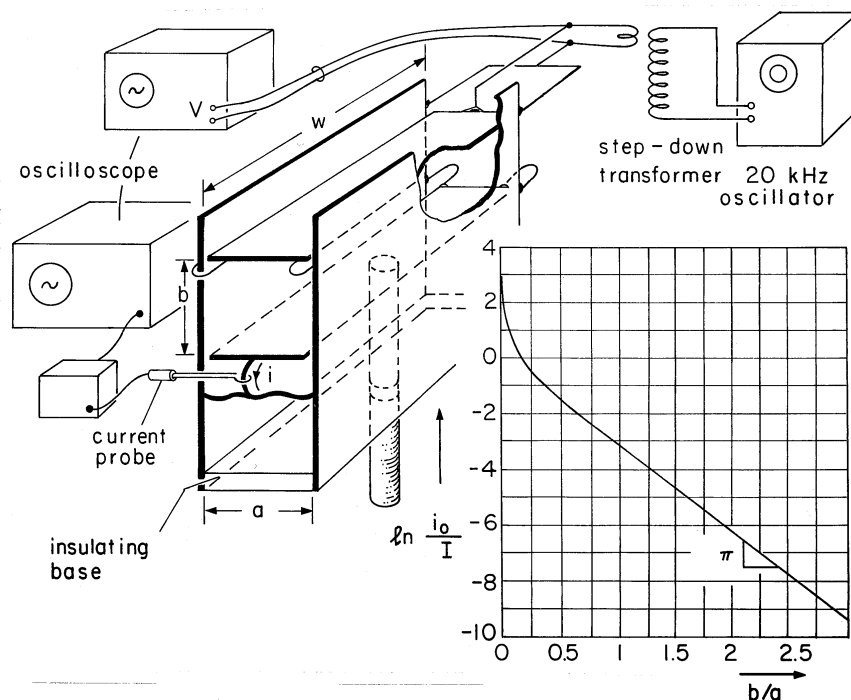
Fig. 8.6.11   Inductive attenuator demonstration.

In a final example, we exemplify how the particular and homogeneous solutions are combined to satisfy boundary conditions while also illustrating how the inductance of a distributed winding is determined.

Example 8.6.4.   Field and Inductance of Distributed Winding Bounded
by Perfect Conductor

The cross-section of a distributed winding of radius a is shown in Fig. 8.6.12. It consists of turns carrying current i in the $+z$ direction at a location (r, ϕ) and returning the current at $(r, -\phi)$ in the $-z$ direction. The density of turns, each carrying the current i in the $+z$ direction for $0 \leq \phi \leq \pi$ and in the $-z$ direction for $\pi < \phi < 2\pi$, is

$$n = n_o |\sin \phi| \tag{25}$$

The total number of wires N in the left-hand half of the coil is

$$N = \int_0^a \int_0^\pi n_o \sin \phi r dr d\phi = n_o a^2 \tag{26}$$

so that the current density is

$$\mathbf{J} = \mathbf{i_z} i n_o \sin \phi = \mathbf{i_z} i \frac{N}{a^2} \sin \phi \tag{27}$$

The windings are very long in the z direction so that effects of the end turns are ignored and the fields taken as independent of z.
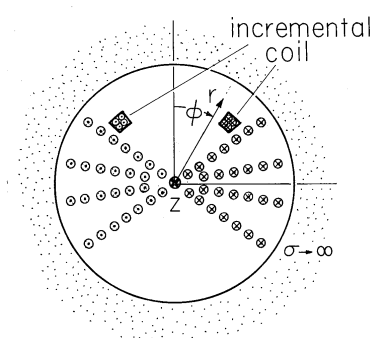
Fig. 8.6.12   Cross-section of two-dimensional distributed winding sur-
rounded by perfectly conducting material. A typical coil consists of wires
carrying current in the $+z$ direction at (r, ϕ) somewhere to the right
$(0 < \phi < \pi)$, and returning it in the $-z$ direction at $(r, -\phi)$ to the left.

The coil is bounded at $r = a$ by a perfect conductor. With the following
steps we determine the field distribution throughout the winding and finally, its
inductance.

The vector potential is z independent and must satisfy Poisson's equation
(8.1.6). In polar coordinates,

$$\frac{1}{r}\frac{\partial}{\partial r}\left(r\frac{\partial A_z}{\partial r} \right) + \frac{1}{r^2}\frac{\partial^2 A_z}{\partial \phi^2} = -\mu_o J_z \tag{28}$$

First we look for a particular solution. If it is to take a product form, inspection
shows that $\sin \phi$ is the appropriate ϕ dependence. Substitution of an r dependence
r^n shows that the equation can be satisfied if $n = 2$. Thus, we have "guessed" a
particular solution.

$$A_{zp} = -\frac{\mu_o N i}{3}\frac{r^2}{a^2}\sin\phi \tag{29}$$

The magnetic flux density normal to the perfectly conducting surface at $r = a$
must be zero, so the total vector potential must be constant there. It follows that
one must add a vector potential with no associated current density in the region
$r < a$, a homogeneous solution A_{zh}. At $r = a$, the homogeneous solution, A_{zh}, must
be the negative of the particular solution, A_{zp}.

$$[A_{zp} + A_{zh}]_{r=a} = 0 \Rightarrow A_{zh}(r = a) = \frac{\mu_o N i}{3}\sin\phi \tag{30}$$

A linear combination of the two solutions to Laplace's equation that have the same
ϕ dependence as this condition is

$$A_{zh} = Cr\sin\phi + \frac{D}{r}\sin\phi \tag{31}$$

The coefficient D must be zero so that the solution is finite at the origin. The
coefficient C is then adjusted to make (31) satisfy the condition of (30). Hence, the
sum of the particular and homogeneous solutions is

$$A_z = -\frac{\mu_o N i}{3}\left[\left(\frac{r}{a}\right)^2 - \frac{r}{a} \right]\sin\phi \tag{32}$$
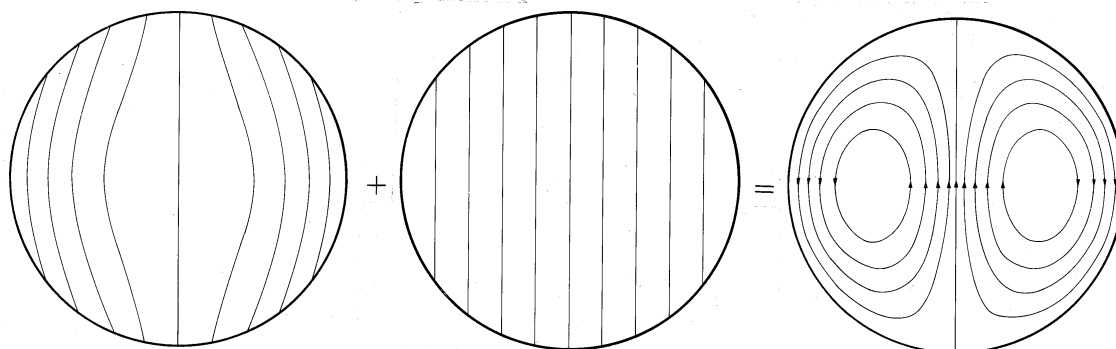
Fig. 8.6.13   Graphical representation of the surfaces of constant A_z for the system of Fig. 8.6.12 as the sum of particular and homogeneous solutions.

A graphical representation of what has been accomplished is given in Fig. 8.6.13, where the surfaces of constant A_z (and hence the lines of field intensity) are shown for the particular, homogeneous, and total solutions.

Each turn of the coil links a different magnetic flux. Thus, to determine the total flux linked by the distribution of turns, it is necessary to carry out an integration. To do this, first observe that the flux linked by the turns with their right legs within the area $rd\phi dr$ in the neighborhood of (r, ϕ) and their left legs within a similar area in the neighborhood of $(r, -\phi)$ is

$$\Phi_\lambda = l[A_z(r, \phi) - A_z(r, -\phi)]n_o \sin \phi rd\phi dr \tag{33}$$

Here, l is the length of the system in the z direction.

The total flux linked by all of the turns is obtained by integrating over all of the turns.

$$\lambda = ln_o \int_0^a \int_0^\pi [A_z(r, \phi) - A_z(r, -\phi)]r \sin \phi d\phi dr \tag{34}$$

Substitution for A_z from (32) and use of (26) then gives

$$\lambda = Li \qquad \text{with} \qquad L \equiv \frac{\pi}{36}l\mu_o N^2 \tag{35}$$

where L will be recognized as the inductance.

8.7 SUMMARY

Just as Chap. 4 was initiated with the representation of an irrotational vector field **E**, this chapter began by focusing on the solenoidal character of the magnetic flux density. Thus, $\mu_o\mathbf{H}$ was portrayed as the curl of another vector, the vector potential **A**.

The determination of the magnetic field intensity, given the current density everywhere, was pursued first using the vector potential. The integration of the

vector Poisson's equation for $\mathbf{A}$ was the first of many exploitations of analogies between EQS and MQS descriptions. In Cartesian coordinates, the superposition integral for $\mathbf{A}$, (8.1.8) in Table 8.7.1, has components that are analogous to the scalar potential superposition integral, (4.5.3), from Table 4.9.1. Similarly, the two-dimensional superposition integral, (8.1.14), has as its analog (4.5.20) from Table 4.9.l.

Especially if a computer is to be used, it is often most practical to work directly with the magnetic field intensity. The Biot-Savart law, (8.2.7) in Table 8.7.1, gives $\mathbf{H}$ directly as an integration over the given distribution of current density.

In many applications, the current distribution can be approximated by piece-wise continuous straight-line segments. In this case, the total field is conveniently represented by the superposition of contributions given by (8.2.22) in Table 8.7.1 due to the individual "sticks."

In regions free of current density, $\mathbf{H}$ is not only solenoidal, but also irrotational. Thus, like the electric field intensity of Chap. 4, it can be represented by a scalar potential Ψ, $\mathbf{H} = -\nabla\Psi$. The magnetic scalar potential is, in general, discontinuous across a surface carrying a surface current density. It is its normal derivative that is continuous. The scalar potential provides an elegant representation of the fields in free space regions surrounding current loops. The superposition integral, (8.3.12) in Table 8.7.1, is written in terms of the solid angle Ω.

Through the combined effects of Faraday's law, flux continuity, and Ohm's law, currents are induced in a conductor by a time-varying magnetic field. In a perfect conductor, these currents are on the surface, distributed in such a way as to shield the magnetic field out of the conductor. As a result, the normal component of the magnetic flux density must be zero on the surface of a perfect conductor.

Although useful for representing any solenoidal field, the vector potential is especially useful in the situations summarized by Table 8.7.2. It is especially convenient for describing systems with perfectly conducting boundaries. In two dimensions, the boundary condition on a perfect conductor is satisfied by making the vector potential constant on the boundary. The approaches of Chaps. 4 and 5 apply equally well to solving MQS boundary value problems involving perfect conductors. In fact, the two-dimensional EQS and MQS configurations of perfect conductors in free space, exemplified by the configurations of Figs. 4.7.2 and 8.6.7, were found to be duals. Formally, the solution for $\mathbf{H}$ follows from that for $\mathbf{E}$ by identifying $\Phi \rightarrow A_z$, $\rho/\epsilon_o \rightarrow \mu_o J_z$. However, while the electric field intensity $\mathbf{E}$ is perpendicular to the surfaces of constant Φ, $\mathbf{H}$ is tangential to the surfaces of constant A_z.

The boundary conditions obeyed by the vector potential at surfaces of discontinuity (containing surface currents) reflect the discontinuity in tangential H field and the continuity of the normal flux density. The vector potential itself must be continuous (a discontinuity of $\mathbf{A}$ would imply an infinite $\mathbf{H}$ in the surface)
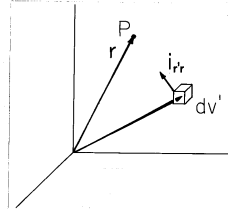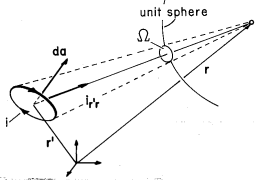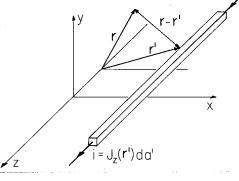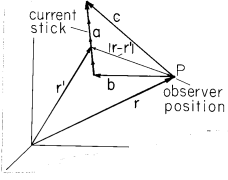
$$(\mathbf{A}^a - \mathbf{A}^b) = 0 \tag{1}$$

where Ampère's continuity condition

$$\mathbf{n} \times [(\nabla \times \mathbf{A})^a - (\nabla \times \mathbf{A})^b] = \mu_o \mathbf{K} \tag{2}$$

requires that *curl* $\mathbf{A}$ have discontinuous tangential components. The condition that $\mathbf{A}$ be continuous, (1), guarantees the continuity of the normal flux density. [According to (1), the integral of $\mathbf{A} \cdot d\mathbf{s}$ around an incremental closed contour lying on one

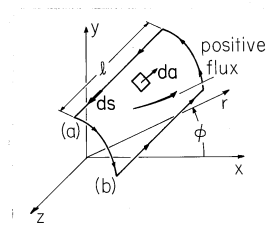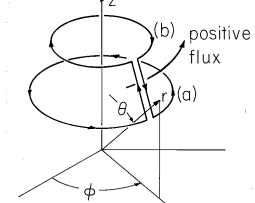**TABLE 8.7.1**

Three-dimensional vector potential $$\mathbf{A}(\mathbf{r}) = \frac{\mu_o}{4\pi} \int_{V'} \frac{\mathbf{J}(\mathbf{r}')dv'}{|\mathbf{r} - \mathbf{r}'|}$$ Three-dimensional magnetic field intensity (Biot-Savart law) $$\mathbf{H} = \frac{1}{4\pi} \int_{V'} \frac{\mathbf{J}(\mathbf{r}') \times \mathbf{i}_{r'r}}{|\mathbf{r} - \mathbf{r}'|^2} dv'$$	(8.1.8) (8.2.7)	
$$\Psi(\mathbf{r}) = \frac{i}{4\pi}\Omega$$ $$\Omega \equiv \int_S \frac{\mathbf{i}_{r'r} \cdot d\mathbf{a}'}{|\mathbf{r}-\mathbf{r}'|^2}$$	(8.3.12) (4.5.29)	
Two-dimensional vector potential $$A_z = -\frac{\mu_o}{2\pi} \int_{S'} \ln\left(\frac{|\mathbf{r} - \mathbf{r}'|}{r_o}\right) \cdot J_z(\mathbf{r}')da'$$	(8.1.14)	
Current "Stick" field $$\mathbf{H} = \frac{i}{4\pi} \frac{\mathbf{c} \times \mathbf{a}}{|\mathbf{c} \times \mathbf{a}|^2} \left(\frac{\mathbf{a} \cdot \mathbf{c}}{|c|} - \frac{\mathbf{a} \cdot \mathbf{b}}{|b|}\right)$$	(8.2.22)	

side of the surface is equal to that on the other. Thus, the normal flux which each of these integrals represents, is the same as well.]

In fluid mechanics, the scalar A_z would be called a "stream-function", because in two dimensions, lines of constant vector potential constitute the flux lines. In axisymmetric configurations, the flux lines are lines of constant Λ_s, as defined in Table 8.7.2. Of course, a similar representation can be used for any solenoidal vector. For example, an expression for the two-dimensional lines of electric field intensity in a region free of charge density could be obtained by finding a vector potential representation of **E**. Thus, in these special cases, the vector potential is convenient for plotting any solenoidal field.

The electric potential Φ of EQS systems, evaluated on the surface of a perfectly

TABLE 8.7.2

Two-Dimensional cartesian coordinates	Eq. No.	
$\mathbf{A} = A_z(x,y)\mathbf{i_z}$	(8.6.3)	
$\mu_o\mathbf{H} = \dfrac{\partial A_z}{\partial y}\mathbf{i_x} - \dfrac{\partial A_z}{\partial x}\mathbf{i_y}$	(8.6.4)	
$\lambda = l(A_z^a - A_z^b)$	(8.6.5)	
Two-dimensional polarcoordinates $\mathbf{A} = A_z(r,\phi)\mathbf{i_z}$		
$\mu_o\mathbf{H} = \dfrac{1}{r}\dfrac{\partial A_z}{\partial \phi}\mathbf{i_r} - \dfrac{\partial A_z}{\partial r}\mathbf{i_\phi}$	(8.6.7)	
$\lambda = l(A_z^a - A_z^b)$	(8.6.5)	
Axisymmetric spherical coordinates $\mathbf{A} = A_\phi(r,\theta)\mathbf{i_\phi}$	(8.6.6)	
$\mu_o\mathbf{H} = \dfrac{1}{2\pi r^2 \sin\theta}\left(\dfrac{\partial \Lambda_s}{\partial \theta}\mathbf{i_r} - r\dfrac{\partial \Lambda_s}{\partial r}\mathbf{i_\phi}\right)$		
$\Lambda_s \equiv 2\pi r \sin\theta A_\phi$	(8.6.8)	
$\lambda = \Lambda_s^a - \Lambda_s^b$	(8.6.7)	

conducting capacitor electrode, can be used to evaluate the terminal voltage. The vector potential is similarly related to the terminal characteristics of a lumped parameter element, this time an inductor. Indeed, we found in Sec. 8.6 that the flux per unit length linked by a pair of conductors in two dimensions was simply the difference of vector potentials evaluated on the two conductors. In Sec. 8.4, we found that the terminal voltage is the time rate of change of this flux linkage.

The division of the field into particular and homogeneous parts makes possible a number of different approaches to obtaining the total field. The particular part can be obtained using the vector potential, using the Biot-Savart law, or by superimposing the fields of thin coils represented in terms the scalar magnetic potential. The homogeneous solution is both irrotational and solenoidal, so it is possible to use either the vector or the scalar potential to represent this part of the field everywhere. The vector potential helps determine the net flux, as required for calculating the inductance, but is of limited usefulness for three-dimensional configurations. The scalar potential does not directly portray the net flux, but does generally apply to three-dimensional configurations.

P R O B L E M S

8.1 The Vector Potential and the Vector Poisson Equation

8.1.1   A solenoid has radius a, length d, and turns N, as shown in Fig. 8.2.3. The length d is much greater than a, so it can be regarded as being infinite. It is driven by a current i.

   (a) Show that Ampère's differential law and the magnetic flux continuity law [(8.0.1) and (8.0.2)], as well as the associated continuity conditions [(8.0.3) and (8.0.4)], are satisfied by an interior magnetic field intensity that is uniform and an exterior one that is zero.
   (b) What is the interior field?
   (c) $\mathbf{A}$ is continuous at $r = a$ because otherwise the $\mathbf{H}$ field would have a singularity. Determine $\mathbf{A}$.

8.1.2*   A two-dimensional magnetic quadrupole is composed of four line currents of magnitudes i, two in the positive z direction at $x = 0$, $y = \pm d/2$ and two in the negative z direction at $x = \pm d/2, y = 0$. (With the line charges representing line currents, the cross-section is the same as shown in Fig. P4.4.3.) Show that in the limit where $r \gg d$, $A_z = -(\mu_o i d^2/4\pi)(r^{-2}) \cos 2\phi$. (Note that distances must be approximated accurately to order d^2.)

8.1.3   A two-dimensional coil, shown in cross-section in Fig. P8.1.3, is composed of N turns of length l in the z direction that is much greater than the width w or spacing d. The thickness of the windings in the y direction is much less than w and d. Each turn carries the current i. Determine $\mathbf{A}$.
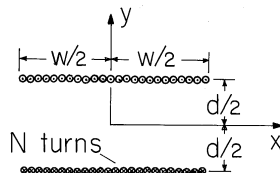

Fig. P8.1.3

8.2 The Biot-Savart Superposition Integral

8.2.1*   The washer-shaped coil shown in Fig. P8.2.1 has a thickness Δ that is much less than the inner radius b and outer radius a. It supports a current density $\mathbf{J} = J_o \mathbf{i}_\phi$. Show that along the z axis,

$$\mathbf{H} = \frac{\Delta J_o \mathbf{i_z}}{2} \left[\frac{b}{\sqrt{b^2 + z^2}} - \frac{a}{\sqrt{a^2 + z^2}} + ln \frac{(a + \sqrt{a^2 + z^2})}{(b + \sqrt{b^2 + z^2})} \right] \tag{a}$$
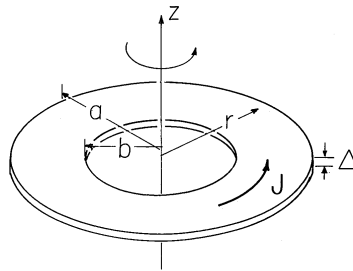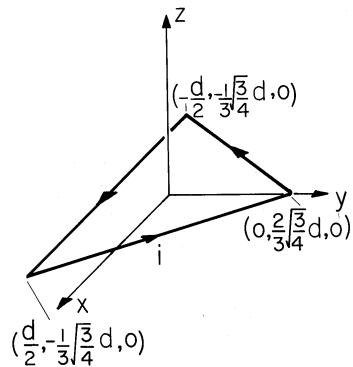
Fig. P8.2.1

Fig. P8.2.5

8.2.2* A coil is wound so that the wire forms a spherical shell of radius R with the wire essentially running in the ϕ direction. With the wire driven by a current source, the resulting current distribution is a surface current at $r = R$ having the density $\mathbf{K} = K_o \sin\theta \mathbf{i}_\phi$, where K_o is a given constant. There are no other currents. Show that at the center of the coil, $\mathbf{H} = (2K_o/3)\mathbf{i_z}$.

8.2.3 In the configuration of Prob. 8.2.2, the surface current density is uniformly distributed, so that $\mathbf{K} = K_o \mathbf{i}_\phi$, where K_o is again a constant. Find $\mathbf{H}$ at the center of the coil.

8.2.4 Within a spherical region of radius R, the current density is $\mathbf{J} = J_o \mathbf{i}_\phi$, where J_o is a given constant. Outside this region is free space and no other sources of $\mathbf{H}$. Determine $\mathbf{H}$ at the origin.

8.2.5* A current i circulates around a loop having the shape of an equilateral triangle having sides of length d, as shown in Fig. P8.2.5. The loop is in the $z = 0$ plane. Show that along the z axis,

$$\mathbf{H} = i\sqrt{3/4}\frac{d^2\mathbf{i_z}}{4\pi}\left(z^2 + \frac{d^2}{12}\right)^{-1}\left(\frac{d^2}{3} + z^2\right)^{-1/2} \qquad (a)$$

8.2.6 For the two-dimensional coil of Prob. 8.1.3, use the Biot-Savart superposition integral to find $\mathbf{H}$ along the x axis.

8.2.7* Show that $\mathbf{A}$ induced at point P by the current stick of Figs. 8.2.5 and 8.2.6 is

$$\mathbf{A} = \frac{\mu_o i}{4\pi} \frac{\mathbf{a}}{|\mathbf{a}|} ln \left[\frac{\frac{\mathbf{c} \cdot \mathbf{a}}{|\mathbf{a}|} + |\mathbf{c}|}{\frac{\mathbf{b} \cdot \mathbf{a}}{|\mathbf{a}|} + |\mathbf{b}|} \right] \qquad (a)$$

8.3 The Scalar Magnetic Potential

8.3.1 Evaluate the H field on the axis of a circular loop of radius R carrying a current i. Show that your result is consistent with the result of Example 8.3.2 at distances from the loop much greater than R.

8.3.2 Determine Ψ for two infinitely long parallel thin wires carrying currents i in opposite directions parallel to the z axis of a Cartesian coordinate system and located along $x = \pm a$. Show that the lines $\Psi = \mathrm{const}$ in the $x - y$ plane are circles.

8.3.3 Find the scalar potential on the axis of a stack of circular loops (a coil) of N turns and length l using 8.3.12 for an individual turn, integrating over all the turns. Find $\mathbf{H}$ on the axis.

8.4 Magnetoquasistatic Fields in the Presence of Perfect Conductors

8.4.1* A current loop of radius R is at the center of a conducting spherical shell having radius b. Assume that $R \ll b$ and that $i(t)$ is so rapidly varying that the shell can be taken as perfectly conducting. Show that in spherical coordinates, where $R \ll r < b$

$$\mathbf{H} = \frac{i\pi R^2}{4\pi} \left[2\cos\theta \left(\frac{1}{r^3} - \frac{1}{b^3} \right) \mathbf{i_r} + \sin\theta \left(\frac{1}{r^3} + \frac{2}{b^3} \right) \mathbf{i_\theta} \right] \qquad (a)$$

8.4.2 The two-dimensional magnetic dipole of Example 8.1.2 is at the center of a conducting shell having radius $a \gg d$. The current $i(t)$ is so rapidly varying that the shell can be regarded as perfectly conducting. What are Ψ and $\mathbf{H}$ in the region $d \ll r < a$?

8.4.3* The cross-section of a two-dimensional system is shown in Fig. P8.4.3. A magnetic flux per unit length $s\mu_o H_o$ is trapped between perfectly conducting plane parallel plates that extend to infinity to the left and right. At the origin on the lower plate is a perfectly conducting half-cylinder of radius R.

(a) Show that if $s \gg R$, then

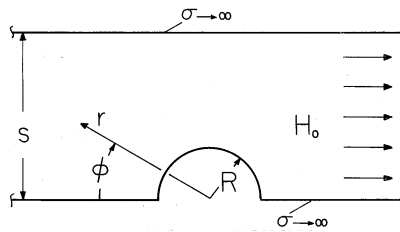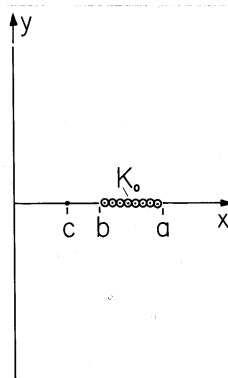$$\Psi = H_o R \left(\frac{r}{R} + \frac{R}{r} \right) \cos\phi \qquad (a)$$

Fig. P8.4.3

Fig. P8.4.6

    (b) Show that a plot of **H** would appear as in the left half of Fig. 8.4.2 turned on its side.

8.4.4 In a three-dimensional version of that shown in Fig. P8.4.3, a perfectly conducting hemispherical bump of radius $s \gg R$ is attached to the lower of two perfectly conducting plane parallel plates. The hemisphere is centered at the origin of a spherical coordinate system such as in Fig. P8.4.3, with $\phi \to \theta$. The magnetic field intensity is uniform far from the hemisphere. Determine Ψ and **H**.

8.4.5[*] Running from $z = -\infty$ to $z = +\infty$ at $(x, y) = (0, -h)$ is a wire. The wire is parallel to a perfectly conducting plane at $y = 0$. When $t = 0$, a current step $i = Iu_{-1}(t)$ is applied in the $+z$ direction to the wire.

    (a) Show that in the region $y < 0$,

$$\mathbf{H} = \frac{i}{2\pi} \left\{ \frac{-(y+h)\mathbf{i_x} + x\mathbf{i_y}}{[x^2 + (y+h)^2]} + \frac{(y-h)\mathbf{i_x} - x\mathbf{i_y}}{[x^2 + (y-h)^2]} \right\} \qquad \text{for} \quad t > 0 \qquad (a)$$

    (b) Show that the surface current density at $y = 0$ is $K_z = -ih/\pi(x^2 + h^2)$.

8.4.6 The cross-section of a system that extends to infinity in the $\pm z$ directions is shown in Fig. P8.4.6. Surrounded by free space, a sheet of current has
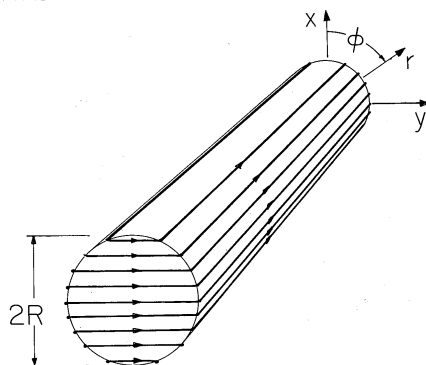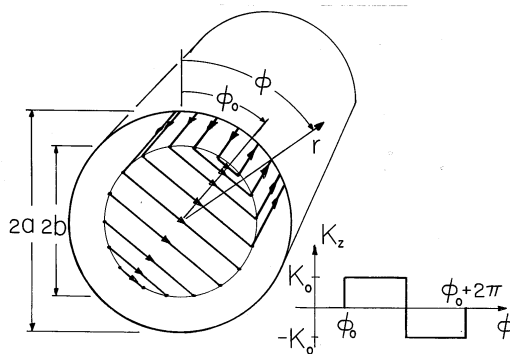
Fig. P8.5.1

Fig. P8.5.2

the surface current density $K_o\mathbf{i_z}$ uniformly distributed between $x = b$ and $x = a$. The plane $x = 0$ is perfectly conducting.

(a) Determine Ψ in the region $0 < x$.
(b) Find $\mathbf{K}$ in the plane $x = 0$.

8.5 Piece-Wise Magnetic Fields

8.5.1[*]   The cross-section of a cylindrical winding is shown in Fig. P8.5.1. As projected onto the $y = 0$ plane, the number of turns per unit length is constant and equal to $N/2R$. The cylinder can be modeled as infinitely long in the axial direction.

(a) Given that the winding carries a current i, show that

$$\Psi = \frac{Ni}{4} \begin{cases} (R/r)\cos\phi; & R < r \\ -(r/R)\cos\phi; & r < R \end{cases} \qquad (a)$$

and that therefore

$$\mathbf{H} = \frac{Ni}{4R} \begin{cases} (R/r)^2[\cos\phi\mathbf{i_r} + \sin\phi\mathbf{i_\phi}]; & R < r \\ [\cos\phi\mathbf{i_r} - \sin\phi\mathbf{i_\phi}]; & r < R \end{cases} \qquad (b)$$

(b) Show that the inductance per unit length of the winding is $L = \pi\mu_o N^2/8$.

8.5.2   The cross-section of a rotor, coaxial with a perfectly conducting "magnetic shield," is shown in Fig. P8.5.2. Windings consisting of N turns per unit peripheral length are distributed uniformly at $r = b$ so that at a given instant in time, the surface current distribution is as shown. At $r = a$, there is the inner surface of a perfect conductor. The system is very long in the z direction.

(a) What are the continuity conditions on Ψ at $r = b$ and the boundary condition at $r = a$?
(b) Find Ψ, and hence $\mathbf{H}$, in regions (a) and (b) outside and inside the winding, respectively.
(c) With the understanding that the rotor is wound using one wire, so that each turn is in series with the next and a wire carrying the current in the $+z$ direction at ϕ returns the current in the $-z$ direction at $-\phi$, what is the inductance of the rotor coil? Why is it independent of the rotor position ϕ_o?

8.6 Vector Potential

8.6.1[*]   In Example 1.4.1, the magnetic field intensity is determined to be that given by (1.4.7). Define A_z to be zero at the origin.

(a) Show that if H_ϕ is to be finite in the neighborhood of $r = R$, A_z must be continuous there.
(b) Show that $\mathbf{A}$ is given by

$$\mathbf{A} = -\mathbf{i_z}\frac{\mu_o J_o R^2}{3} \begin{cases} \frac{1}{3}(r/R)^3; & r < R \\ ln(r/R) + \frac{1}{3}; & r > R \end{cases} \qquad (a)$$

(c) The loop designated by C' in Fig. 1.4.2 has a length l in the z direction, an inner leg at $r = 0$, and an outer leg at $r = a > R$. Use $\mathbf{A}$ to show that the flux linked is

$$\lambda = -lA_z(a) = \frac{\mu_o J_o R^2 l}{3}\left[ln(a/R) + \frac{1}{3}\right] \qquad (b)$$

8.6.2   For the configuration of Prob. 1.4.2, define A_z as being zero at the origin.

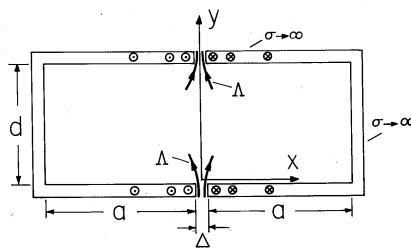(a) Determine A_z in the regions $r < b$ and $b < r < a$.

Fig. P8.6.5

(b) Use **A** to determine the flux linked by a closed rectangular loop having length l in the z direction and each of its four sides in a plane of constant ϕ. Two of the sides are parallel to the z axis, one at radius $r = c$ and the other at $r = 0$. The other two, respectively, join the ends of these segments, running radially from $r = 0$ to $r = c$.

8.6.3* In cylindrical coordinates, $\mu_o\mathbf{H} = \mu_o[H_r(r,z)\mathbf{i_r} + H_z(r,z)\mathbf{i_z}]$. That is, the magnetic flux density is axially symmetric and does not have a ϕ component.

(a) Show that
$$\mathbf{A} = [\Lambda_c(r,z)/r]\mathbf{i_\phi} \qquad (a)$$

(b) Show that the flux passing between contours at $r = a$ and $r = b$ is
$$\lambda = 2\pi[\Lambda_c(a) - \Lambda_c(b)] \qquad (b)$$

8.6.4* For the inductive attenuator considered in Example 8.6.3 and Demonstration 8.6.2:

(a) derive the vector potential, (20), without identifying this MQS problem with its EQS counterpart.
(b) Show that the current is as given by (21).
(c) In the limit where $b/a \gg 1$, show that the response has the dependence on b/a shown in the plot of Fig. 8.6.11.
(d) Show that in the opposite limit, where $b/a \ll 1$, the total current in the lower plate (21) is consistent with a magnetic field intensity between the upper and lower plates that is uniform (with respect to y) and hence equal to $(\Lambda/b\mu_o)\mathbf{i_x}$. Note that

$$\sum_{\substack{n=1 \\ \text{odd}}}^{\infty} \frac{1}{n^2} = \frac{\pi^2}{8} \qquad (a)$$

8.6.5 Perfectly conducting electrodes are composed of sheets bent into the shape of ⊔'s, as shown in Fig. P8.6.5. The length of the system in the z direction is very large compared to the length $2a$ or height d, so the fields can be
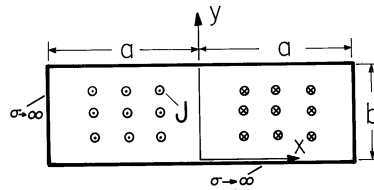
Fig. P8.6.6

regarded as two dimensional. The insulating gaps have a width Δ that is small compared to all dimensions. Passing through these gaps is a magnetic flux (per unit length in the z direction) $\Lambda(t)$. One method of solution is suggested by Example 6.6.3.

  (a) Find $\mathbf{A}$ in regions (a) and (b) to the right and left, respectively, of the plane $x = 0$.
  (b) Sketch $\mathbf{H}$.

8.6.6* The wires comprising the winding shown in cross-section by Fig. P8.6.6 carry current in the $-z$ direction over the range $0 < x < a$ and return this current over the range $-a < x < 0$. These windings extend uniformly over the range $0 < y < b$. Thus, the current density in the region of interest is $\mathbf{J} = -in_o \sin(\pi x/a)\mathbf{i_z}$, where i is the current carried by each wire and $|n_o \sin(\pi x/a)|$ is the number of turns per unit area. This region is surrounded by perfectly conducting walls at $y = 0$ and $y = b$ and at $x = -a$ and $x = a$. The length l in the z direction is much greater than either a or b.

  (a) Show that

$$\mathbf{A} = \mathbf{i_z}\mu_o in_o(a/\pi)^2 \sin\left(\frac{\pi x}{a}\right)\left[\frac{\cosh\frac{\pi}{a}\left(y - \frac{b}{2}\right)}{\cosh\left(\frac{\pi b}{2a}\right)} - 1\right] \qquad (a)$$

  (b) Show that the inductance of the winding is

$$L = 2\mu_o n_o^2 l \frac{a^4}{\pi^3}\left[\left(\frac{\pi b}{2a}\right) - \tanh\left(\frac{\pi b}{2a}\right)\right] \qquad (b)$$

  (c) Sketch $\mathbf{H}$.

8.6.7 In the configuration of Prob. 8.6.6, the rectangular region is uniformly filled with wires that all carry their current in the z direction. There are n_o of these wires per unit area. The current carried by each wire is returned in the perfectly conducting walls.

  (a) Determine $\mathbf{A}$.
  (b) Assume that all the wires are connected to the wall by a terminating plate at $z = l$ and that each is driven by a current source $i(t)$ in the plane $z = 0$. Note that it has been assumed that each of these current

sources is the same function of time. What is the voltage $v(x, y, t)$ of these sources?

8.6.8 In the configuration of Prob. 8.6.6, the turns are uniformly distributed. Thus, n_o is a constant representing the number of wires per unit area carrying current in the $-z$ direction in the region $0 < x$. Assume that the wire carrying current in the $-z$ direction at the location (x, y) returns the current at $(-x, y)$.

    (a) Determine **A**.
    (b) Find the inductance L.